Development of a Model-Specific Tuning Methodology for Frontal Impact Rib Fracture Injury Risk Assessment for Multibody Human Body Models

Sydney Koerber, Katarzyna Rawska, Richard Lancashire, Freerk Bosma, Bronislaw Gepner, Jason Forman

Abstract Occupant models require a means to translate between model measurements and injury risk. Rib fracture injury risk functions have been developed for ATDs and some human body finite element models (HBMs). This study develops frontal-impact rib fracture injury risk functions (IRFs) for use with Simcenter Madymo's Active Human Model (AHM). One hundred and seventy simulations were performed in 13 load cases, with each simulation matched to a specific past PMHS test. Injury risk functions were developed for predicting the risk of 3+ rib fractures, and 7+ rib fractures. The maximum chest deflection from the four measurement sites in the AHM was selected as the final predictor, due to its predictive fit and its low sensitivity to changes in loading location. This process may be repeated to refit the injury risk function when future updates are made to the model, allowing distribution of the injury risk function for use with the specific model for which it was tuned. These results demonstrate that it is possible to fit model-specific injury risk functions for human body models that use different modeling methodologies, facilitating flexibility in choice of human body model to fit the needs of various applications.

Keywords Rib fracture; thorax; human body model; Madymo; injury risk function

I. INTRODUCTION

Rib fractures are among the most common types of AIS3+ injuries in frontal collisions [1]. As with many other injury types, most cases of rib fractures occur in collisions of relatively low severity [2-3] due to the dominance of low-to-moderate speed collisions in the distribution of collision exposures. The vast majority of collisions occur with low-to-moderate changes in speed (ΔV). The median ΔV of frontal-impact tow-away collisions is just 18 km/h [2]. The per-crash risk of AIS 3+ injuries in such high-exposure, lower-speed collisions is less than 5% [2]. However, when the high exposure is crossed with that risk (as low as it is), the net result is that most rib fracture injuries occur in low-speed collisions where the per-crash risk is very low. The median ΔV of frontal-impact tow-away collisions that result in AIS 3+ rib fractures is just 38 km/h [2]. This presents a challenge, in that further improvements to drive down rib fracture injury will likely require safety systems that can further reduce risk in scenarios where the injury risk is already quite low (but the exposure is very high).

For any human body model to be useful as a tool for restraint system design, we must have an injury risk function relating the model's output measures to the risk of rib fracture injury (ideally capable of predicting the risk of different severities of rib fracture injury). This is likely not as simple as applying an injury risk function previously developed for a dummy or another model. Due to the wide bounds found in typical biofidelity corridors, two different models can both be judged biofidelic, while still exhibiting differences in response that may result in different injury prediction if a common IRF were to be applied. To accommodate this, Forman et al. [22] suggested a process whereby IRFs should be tuned for specific FE-based human body models, seeking to arrive at harmonized injury risk prediction despite differences in model responses. That study developed a methodology to tune frontal-impact rib fracture injury risk functions using a suite of 170 simulations (in 13 individual load cases) matched to past tests with postmortem human surrogates (PMHS). This approach is similar to past methods to tune rib fracture injury risk functions for specific crash test dummies, where tests were performed with the dummies matching conditions used in past PMHS tests, and then regression models were developed relating the dummy measures to injuries observed in the matched PMHS tests [23]. When applied to HBMs, this methodology allows the flexibility for different HBMs to take different modeling approaches, harmonizing injury prediction by developing unique injury risk functions tuned for each human body model. That

study developed the load case simulations in an FE environment (LS-Dyna, ANSYS Inc, Canonsburg, PA), and demonstrated the methodology by applying to two FE HBMs (THUMS v.4.1 and GHBMC-M50O v.6.0), developing model-specific IRFs based on rib strain.

The goal of this study is to modify the framework developed by Forman et al. [22] to develop a methodology to tune frontal-impact rib fracture injury risk functions for use with analytical multi-body models such as the SimCenter Madymo Active Human Model ("Madymo AHM"; Siemens Industry Software, Leuven). This required rebuilding the thirteen IRF-tuning load cases of Forman et al. [22] in a multi-body environment. Each environment was set up and run with the same inputs as the THUMS and GHBMC simulations described by Forman et al. [22]. The environment was tuned (belt-refitting, AHM initial position) within reasonable bounds according to the original literature. To demonstrate this methodology, the response of the Madymo AHM was then examined in each load case to critically review for the reasonableness of the biofidelity, and to identify output measures that may be suitable bases for an IRF. The model was then subjected to the full battery of IRF-tuning simulations developed by Forman et al. [22]. A collection of candidate output measures were then used to fit possible IRFs, which were then compared to arrive at the final recommended IRF.

II. METHODS

The frontal impact rib fracture IRF tuning methodology developed by Forman et al. [22] was applied to the Madymo AHM version 3.3. The AHM is a multi-body-based model of the human body designed for dynamic automobile safety simulation applications [46]. Its whole-body response and thoracic response have been evaluated against several impactor and sled-type loading modes, including cases with seatbelt and airbag loading [25-26;37-45].

The first step of the IRF tuning process was to translate the 13 impactor and table-top loading environments described by Forman et al. [22], Table 1, into the Madymo environment. These consisted of 48 load cases with a Kroell-type impactor (frontal and oblique), 7 load cases with either a straight rigid bar impactor or curved steering-wheel style impactor, 18 table-top cases with a hub-type loader, 16 table-top cases with a distributed belt loader, and 43 table-top cases with single diagonal belt loading, and 38 table-top cases with double diagonal belt loading. The load case simulations are illustrated in Appendix A.

Preliminary Assessment

Preliminary simulations were then performed in each of these load cases to check the general performance of the model, and to identify model outputs that may serve as potential injury prediction measures. This preliminary assessment sought to determine if the model exhibited a reasonable response (in terms of stability, penetration, general interaction with the environment, etc.), prior to proceeding with the large-scale simulation sweep for IRF tuning. This preliminary assessment also facilitated examination of the candidate model output measures to identify which may potentially be suitable for injury prediction. For example, the chest deflection output measures were examined relative to the loading locations in the various load cases, to observe whether or not they may be susceptible to sensitivity in loading location and/or loading pattern.

For this preliminary assessment, the Madymo AHM was exercised in the loading modes of Table I using the average inputs applied in the matching PMHS tests. Chest deflection results were output for four measurement locations, positioned over a vertical span on the centerline of the chest (Figure 1).

TABLE 1
IMPACTOR AND TABLETOP CASES USED FOR INJURY RISK FUNCTION FITTING

Type	PMHS Test Series	Loading Condition	No. of PMHS	Total no. of Tests	No. of tests with 3+ rib fractures
Impactor	Kroell 1971, 1974	Rigid Hub	38	38	30
	Horsch 1988	Rigid Hub	3	3	3
	Yoganandan 1997	Rigid Hub	7	7	5
	Hardy 2001	Rigid Bar	3	3	3
	Shaw 2004	Rigid Steeling Wheel Rim	4	4	2

	Kent 2004	Rigid Hub	15	18	3
		Distributed Belt		16	1
		Single Diagonal Belt		18	2
		Double Diagonal belt		15	2
Tabletop	Forman 2005	Load Limited Double Diagonal Belt	3	23	2
	Salzar 2009	Single Diagonal Belt	3	6	0
	Cesari 1990, 1994	Single Diagonal Belt	17	17	14
	Kemper 2011	Single Diagonal Belt	2	2	2

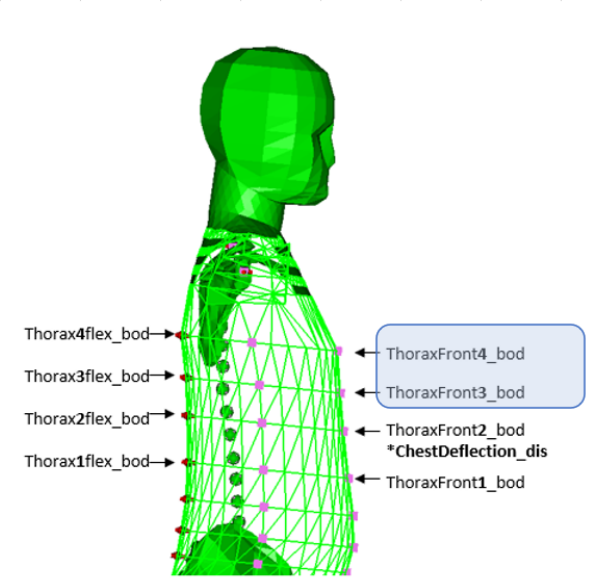

Figure 1: Madymo AHM chest deflection output locations. Typical mid-sternal hub impact location illustrated for context.

Matched-Case Simulations and IRF Fitting

Following preliminary examination of the model and the potential suitability of its chest deflection measures, the model was exercised following the rib fracture IRF tuning methodology of Forman et al. [22]. The rib fracture IRF tuning method of Forman et al. [22] is similar in concept to past efforts to develop IRFs for dummies via matched pair testing. In such a method, simulations are performed with the target model matching prior PMHS tests. The model measurement outputs are then regressed against the injuries observed in each of the matched PMHS tests to develop the IRF. In this process, a critical step is to match the severity of the input loading conditions between the PMHS tests and the matched simulations. The model outputs are then taken at face value, reflecting the inherent characteristics of how the model responds when faced with scenarios that were injurious or non-injurious to the PMHS. Often when such a process is applied to physical occupant models (dummies), however, it is challenging to match the relative severity of loading experienced by each PMHS. Specifically, in fixed-energy, fixed-momentum tests such as impactor tests, the severity of loading of the PMHS can be affected by the mass of the PMHS relative to the impactor, which affects the change in velocity imparted to the PMHS. In simulation, however, this can be accommodated by scaling the impactor mass by the mass of the matched PMHS, so that the HBM experiences a similar change in velocity compared to the matched PMHS. Similarly, most table-top PMHS studies define targets for input loader motion based on a percentage of the initial chest depth of the subject PMHS. Again, this may be readily accommodated in the simulation by adjusting the input loader motions to match the normalized chest compressions experienced in the matched PMHS tests.

By modifying the simulation input conditions as described above, the framework of Forman et al. [22] results in performing a specific individual simulation to match each past PMHS test in the dataset, modifying impactor velocity and scaled impactor mass to match each past impactor PMHS test (Appendix B) and modifying the loader

displacement magnitude normalized by chest depth for the table-top cases.

Following execution of the suite of 170 simulations, regression models were developed to evaluate and compare potential chest injury prediction measures. Based on observations from the preliminary biofidelity assessment described above, the potential chest injury prediction measures included the chest compression at the stock singular Madymo AHM output location, the maximum chest compression among the four Madymo AHM output locations (Figure 1), the average chest compression among those locations, and a linear combination of the average and the maximum difference in chest compression among those locations [23]. These candidate measures were evaluated via General Estimating Equations (GEE) using a logistic formulation with age as a covariate [22-23]. GEE was used because Forman et al. [22] included some cases of repeated tests performed on the same PMHS (i.e., multiple initial low-severity, non-injurious tests, followed by a single high-severity injurious tests). GEE can account for multiple observations from the same PMHS by treating such cases as clustered data [36]. The potential suitability of each candidate measure was then compared via the Area Under the Receiver Operator Curve (AUROC, a measure of classification potential), and the Quasi-likelihood under Independence Model Criterion (QIC; a likelihood-based measure analogous to the AIC, suited for GEE models of clustered data). The potential predictors were then down-selected based on comparison of these measures, as well as practical usability considerations observed in the baseline biofidelity assessments.

Similar to Forman et al. [22], IRFs were fitted for predicting the risk of 3+ rib fractures, and 7+ rib fractures. Age was included as a covariate in all IRFs (Equation 1). Note that by including age as a co-variate in the IRFs, we give the IRFs the flexibility to naturally account for any systematic difference in injury tolerance associated with age, without needing estimate and adjust for the age effects in the underlying data *a priori*.

$$Probability\ of\ Injury = \frac{1}{1 + e^{-q}}$$

$$q = \beta_0 + \beta_1 * deflection(m) + \beta_2 * age(years) \qquad \text{Eq. 1}$$

III. RESULTS

Preliminary Assessments

Illustrations of the model setups and responses for each load case are shown in Appendix A. These preliminary simulations served to refine the setups to ensure proper input condition definitions prior to proceeding to the full battery of simulations (via refining the belt-fitting, AHM initial position, input conditions, etc.). Overall, the model behavior appeared reasonable, fitting within the range of prior PMHS responses/corridors in most load cases. Notable exceptions are the response to steering wheel rim impact [30], and the chest deflection observed in one particular belt loading case [34]. The latter belt use case is a unique legacy case that contained limited published information to utilize in the assessment. The biofidelity deviations observed in case [34] were not observed in the other belt loading cases, suggesting that [34] may not be a strong indicator of the overall biofidelity of the model.

As noted above, another goal of the preliminary simulations was to examine the potential chest deflection outputs to identify possible candidate measures to form the IRF. In examining the potential chest deflection outputs, one key observation was that the location of the maximum chest deflection was sensitive to the particular load case being applied. For example, as shown in Figure 2, in the Kent tabletop hub impact condition, the maximum chest deflection occurred in the 2nd to superior-most chest deflection output location present in the Madymo AHM. The deflection measured in the top-most measurement location was similar, but the deflections measured in inferior locations were substantially less. However, as shown in Figure 3, if the hub is positioned 20 mm lower the maximum chest deflection occurs in the 2nd to inferior-most measurement location (with the deflection in the superior-most measurement location being substantially less). For comparison, the AHM default chest deflection signal (ChestDeflection_dis) is defined as a relative displacement between the Thorax2Front bod and the Thorax2Flex_bod, shown in Figure 2.

Figure 2 shows the chest deflection time history at the 4 chest deflection measurement locations (all located on the mid-sagittal plane). Each level shows different amount of chest deflection, with the Thorax3Front_bod being the highest.

The key conclusion from that observation is that if the injury risk were to be predicted by a singular measure alone (e.g., the stock AHM chest deflection output), there is a chance that predicted risk may be artificially influenced by the location or shape of the loader (in a manner that may reduce its predictive ability). As a result, in addition to examining the stock chest deflection measurement as a candidate predictor ("ChestDeflection_dis"), we also examined the maximum deflection measured among all for output sites as another candidate predictor ("Maximum Chest Deflection"). For completeness, we also examined both the average deflection and the maximum difference in chest deflection as potential predictors, on the chance that injury risk may be best predicted by either the aggregated sum of deflections or the greatest differences in deflections among the measurement sites.

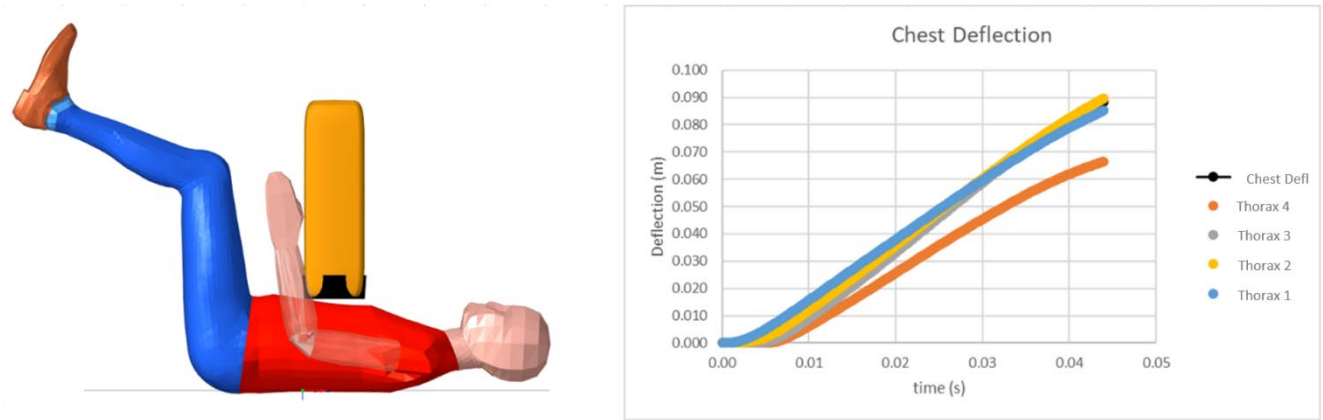

Figure 3: Hub-type loading with the loader positioned 20 mm inferior to the position shown in Figure 2. When the loader is repositioned in this way, the location of the peak chest deflection changes.

Matched-Case Simulations and IRF Fitting

Tables 2 and 3 show the coefficients and diagnostic measures (AUROC and QIC) for the IRFs fit for the four candidate measures. As shown in Table 2, the IRFs based on the maximum chest deflection and the average chest deflection output exhibited the best predictive ability, with similar AUROC and QIC values. Since the fit measures are similar for those two options, we turn to practical considerations to decide the metric on which to focus. All else being equal, the maximum deflection is a simpler term. It also carries less risk of being artificially reduced

under highly concentrated loads (that may cause lesser average deflection by concentrating all the loading in one location). Thus, for simplicity and for consideration of scenarios that may result in highly concentrated deflection, our recommended IRF is the IRF based on the maximum deflection measured among the four measurement sites. These IRFs are shown in Figure 4.

TABLE 2
INJURY RISK FUNCTION FITTING RESULTS FOR 3+ RIB FRACTURES

			Deflection (m)		Age (years)			
Predictor	β0	p	β1	p	β2	p	AUROC	QIC*
'ChestDeflection_dis' Output	-5.0476	0.001	64.7652	6.9E-09	0.0391	0.06	0.872	157
Maximum Chest Deflection	-5.7238	8E-04	73.5518	3.6E-08	0.042	0.064	0.882	152
Average Chest Deflection	-5.6637	9E-04	90.4479	4.8E-08	0.0419	0.068	0.886	153
Maximum Difference	-4.0252	0.003	81.7337	1.7E-10	0.0318	0.092	0.829	168

* A lower QIC value indicates a better model fit.

TABLE 3
INJURY RISK FUNCTION FITTING RESULTS FOR 7+ RIB FRACTURES

			Deflection (m)		Age (years)			
Predictor	β0	p	β1	p	β2	p	AUROC	QIC*
'ChestDeflection_dis' Output	-5.3721	1E-06	45.477	3.7E-08	0.0376	0.006	0.853	151
Maximum Chest Deflection	-5.6927	1E-06	49.5926	3.9E-07	0.0382	0.006	0.862	148
Average Chest Deflection	-5.7814	2E-06	61.7127	4.3E-07	0.0395	0.006	0.866	149
Maximum Difference	-4.81	2E-06	65.1426	6.4E-08	0.033	0.009	0.813	156

* A lower QIC value indicates a better model fit.

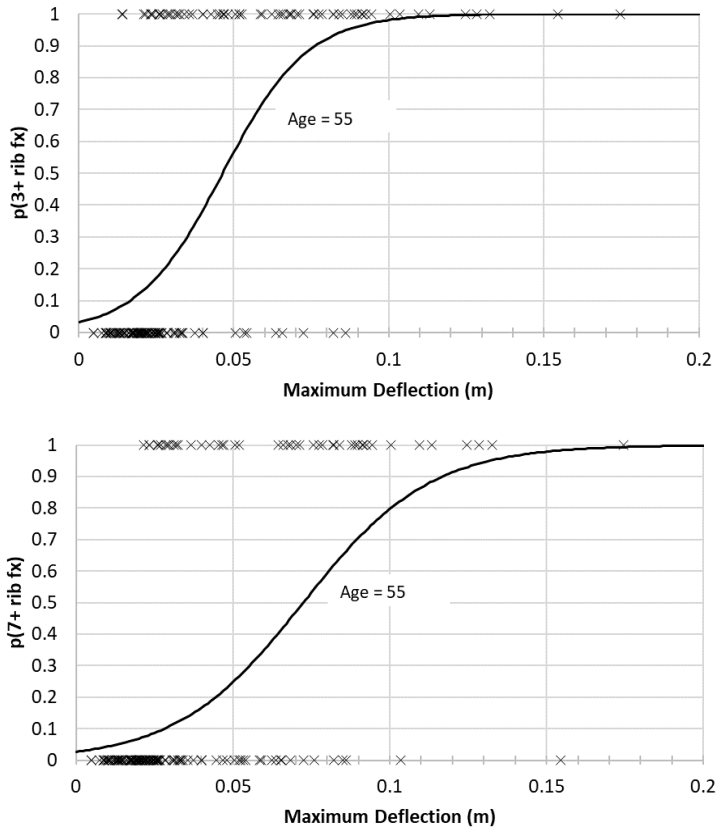

Figure 4: Injury risk functions (calculated for age = 55 years), based on the maximum deflection measured among the four available measurement locations. Top: Function for 3+ rib fractures. Bottom: Function for 7+ rib fractures. Also showing the individual simulation deflection results, designated as injurious or non-injurious based on the matched PMHS tests (shown as X's).

Figure 5 shows bubble-plot style reliability diagrams illustrating the relative predictive ability of the IRFs for each specific load case (comparing the average predicted risk for each load case, to the proportion of PMHS that exhibited the injury of interest for each load case). These plots show reasonable prediction of the overall average risk for most load cases (both impactor and belt loading) that had a high enough number of tests to result in a useful injury proportion estimate. The one notable exception was the belt loading case of [34], which resulted in an underestimation of the risk prediction. As noted above, this deviation was also observed in the baseline biofidelity assessment results, wherein the resulting chest deflection was substantially lower than that reported for the PMHS. Since this was not observed in the other belt loading cases, and since this was a legacy case with limited published information, this may be more of an indicator of the challenge of recreating that case based on the limited information available (and not necessarily a limitation of the model or IRF).

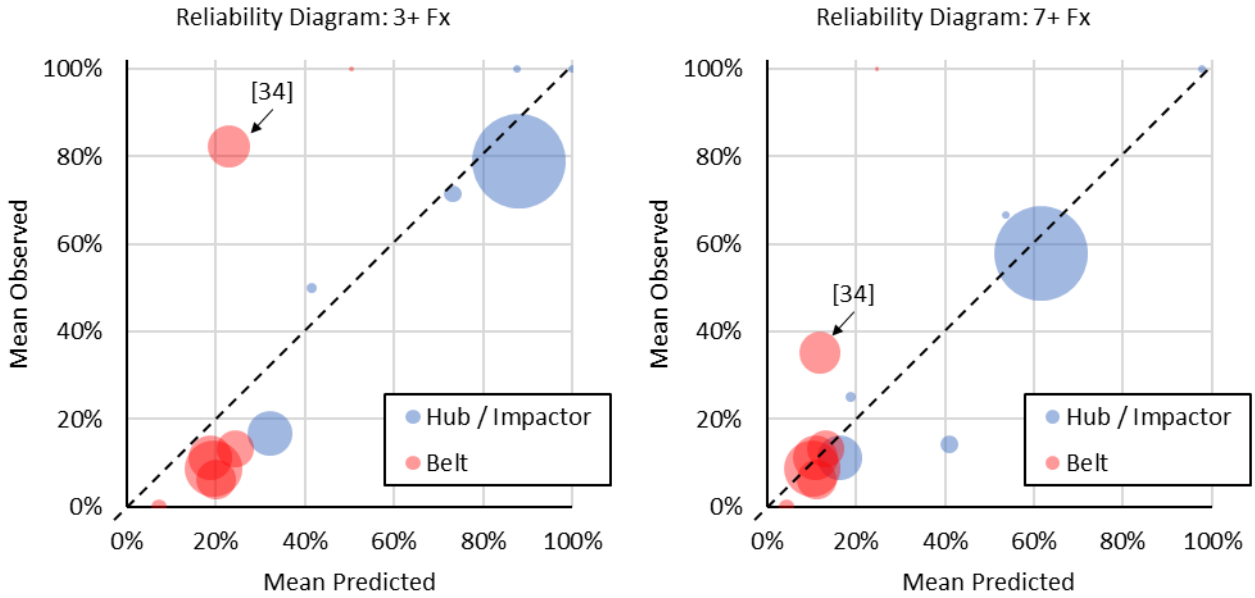

Fig. 5. Reliability diagram bubble plots comparing the average predicted risks for each load case to the proportion of tests with the outcomes of interest. Each circle is a specific load case, with the x-axis showing the average predicted risk for that load case (calculated for the specific age for each matched PMHS). For comparison, the y-axis shows the proportion of PMHS within that load case that exhibited the injury outcome of interest (3+ or 7+ fractures). The dashed line illustrates a 1:1 relationship, which would indicate perfect prediction. The diameter of each bubble is proportional to the number of tests/simulations contained in each specific load case.

IV. Discussion

Thoracic injury prevention is a motivating factor for pursuing adaptive restraint systems. Most rib fracture injuries occur in collisions with ΔVs less than 40 km/h [2]. Dynamically-adaptable restraint systems, capable of producing a softer response with lesser force applied in low speed collisions, have the potential to reduce the risk of rib fracture injury in collisions that occur with high exposure but low per-crash injury risk. Development of such adaptable systems may be best suited to simulation, which can be used not only to optimize the performance of the restraint systems, but also to simulate the potential effects of uncertainty associated with sensing of the collision or occupant characteristics. With this, simulation may fill a role in development of adaptive systems that physical testing cannot accomplish alone, allowing assessment of not only the point effectiveness of such systems but also the robustness of protection provided recognizing potential uncertainty in collision or occupant classification.

Such restraint adaptation and optimization with consideration for multiple sources of uncertainty will require very large-scale simulation studies, potentially incorporating machine learning to allow interpolation between discrete simulations [16]. These simulation studies will challenge the capabilities of FE-based approaches, which will be limited by long computation times. Multi-body-based approaches have the potential to fill the gap between FE tools that require long computation times, and the need for fast-running physics-based models to populate large-scale studies for restraint system adaptation with consideration for collision, occupant, and

sensing uncertainty.

This study demonstrates that, as with other occupant model types, a model-specific rib fracture injury risk function can be tailored for use with an analytical multibody model such as the Madymo AHM. The example IRF developed here is based on the maximum chest deflection measured among the AHM's four measurement locations, mitigating the risk that the injury prediction may be artificially affected by changes in the location where the restraining load is applied (or by local numerical sensitivities and assumptions built into the model). Next steps should include evaluating the model and the IRFs in a range of exemplar use case scenarios (e.g., in-vehicle simulations with a range of collision severities and restraint types) to evaluate the validity of the IRF in cases not used in the IRF fitting [22]. Such an independent validation could be performed using whole-body sled test cases for which PMHS injury reference data are available (checking the model's predictions against the rib fractures observed in the PMHS). Alternatively, an independent validation could include performing simulations in a vehicle environment representative of some portion of collisions occurring in the field, and then comparing the model-based risk predictions to the rate of rib fractures occurring in similar cases in field data. Ideally, such validation exercises should be performed across multiple test cases and loading regimes (frontal, oblique, etc.) to observe the sensitivity of the predictions to changes in the collision and restraint environment.

Current plans for standardized virtual assessment anticipate allowing the flexibility for manufacturers to use the types of models that best fit their needs. This includes not only the specific HBM used, but also the modeling environment/code used. While allowing flexibility in model choice is wise, it also requires methods to ensure that the risks predicted using the various models / codes are consistent. Without harmonization on risk prediction, it is possible that end users may simply select the model that results in the least predicted risk in their application (perhaps inadvertently). Biofidelity assessment alone is not sufficient to harmonize risk prediction. As discussed by Forman et al. [22], due to person-to-person variability, PMHS-based biofidelity corridors are typically wide enough that two HBMs could both be judged as biofidelic yet still exhibit somewhat different responses. Even if such differences in response are relatively small, they have the potential to affect meaningful differences in injury risk prediction due to the non-linear nature of injury risk functions. By tuning IRFs for application to specific HBMs, we open the potential to harmonize injury risk prediction across models while accommodating modest differences in model construction and response.

Finally, the model-specific IRF tuning method applied here has the added benefit that it can accommodate changes and updates to the models for which it is applied. When a model is updated, the IRF tuning process can be repeated to result in similar injury prediction even if the update effects the response of the model. This allows a framework for continuing improvements to the models, without sacrificing continuity in injury risk prediction. Using the suite of 170 test-specific simulations described here, future updates to the Madymo AHM may be accompanied by an updated IRF tuned to the specific model version. Given the fast-running nature of multi-body models, this refitting process can happen very rapidly, rerunning the full battery of simulations and refitting the IRFs in less than a day. This process is not confined to the Madymo platform – it may be adapted for application to any modeling platform (FE, multibody, or others). In fact, the same process could even be applied to even simpler computational occupant models (such as occupant models more akin to dummies) as long as they have a baseline level of biofidelity resulting in a reasonable representation of the restraint interactions and kinematics. In addition, other future work will include adding a set of side-impact load cases to the simulation catalog, to expand the model-specific IRF tuning methodology for application side impact (ideally to identify sets of predictors that work universally in both frontal and side impact). Future efforts should also include developing similar model-specific IRF tuning methodologies for other injury types whose prediction measures may be affected by the specific response of the model (e.g., lumbar, abdomen, and knee-thigh-hip injury, and others).

V. CONCLUSIONS

A methodology to tune frontal-impact rib fracture injury risk functions for multi-body models was developed and demonstrated with the Madymo Active Human Model. This method involves performing a suite of 170 hub impact and table-top chest loading simulations (in 13 specific load case scenarios), matched to previous PMHS tests. Baseline biofidelity simulations found that the model exhibits a reasonably biofidelic thoracic force-deflection response in most of the 13 load cases studied. In those simulations, we also observed that the location of maximum chest deflection is sensitive to the location of the loader. After running the full battery of 170 test-matched simulations, IRFs were fitted using four different chest deflection formulations. Based on quantitative

assessment metrics and practical robustness considerations (i.e., the location sensitivity mentioned above), the final draft IRF is based on the maximum chest deflection measured from the four chest deflection measurement sites available with the AHM. These results suggest that it may be feasible to develop model-specific rib fracture injury risk functions for human body models built in different simulation environments, with different injury metric outputs, by applying the IRF tuning process used here (thus preserving flexibility in model choice to fit the needs of various applications.). Next steps should include validating the predictive ability of such an IRF in in-vehicle use case scenarios, in the context of whole-body kinematics and interaction with the restraint system.

VI. ACKNOWLEDGEMENT

This work was supported by a research grant from Siemens. The opinions presented here are solely those of the authors.

VII. REFERENCES

[1] Forman, J., Poplin, G. S., Shaw, C. G., McMurry, T. L., Schmidt, K., Ash, J., & Sunnevang, C. (2019). Automobile injury trends in the contemporary fleet: Belted occupants in frontal collisions. Traffic Injury Prevention, 20(6), 607-612.

[2] Forman, J. L., & McMurry, T. L. (2018). Nonlinear models of injury risk and implications in intervention targeting for thoracic injury mitigation. Traffic injury prevention, 19(sup2), S103-S108.

[3] Forman, J.L., Ostling, M., Mroz, K., Lubbe, N. (2023). Potential injury criteria for collisions with heavy good vehicles. International Conference on the Enhanced Safety of Vehicles (ESV), Paper No. 23-0334.

[4] Hesseling, R.J., Steinbuch, M., Veldpaus, F.E., Klisch, T., 2006. Feedback control of occupant motion during a crash. International Journal of Crashworthiness 11, 81-96.

[5] Kent, R., Forman, J., Parent, D., & Kuppa, S. (2007, June). Rear seat occupant protection in frontal crashes and its feasibility. In 20th International Conference on the Enhanced Safety of Vehicles (pp. 18-21).

[6] Murad, M., Burley, E., Blackburn, B., 2000. Integrated CAE Modeling of Intelligent Restraint Systems (No. 2000-01-0606). SAE International, Warrendale, PA.

[7] Paulitz, T.J., Blackketter, D.M., Rink, K.K., 2006. Constant force restraints for frontal collisions. Proceedings of the Institution of Mechanical Engineers, Part D: Journal of Automobile Engineering 220, 1177–1189.

[8] Schöneburg, R., Breitling, T., 2005. Enhancement of active and passive safety by future PRE-SAFE systems, in: Proceedings of the 19th International Technical Conference on the Enhanced Safety of Vehicles (ESV).

[9] van der Laan, E.,Veldpaus, F., de Jager, B., Steinbuch, M., 2009. Control-oriented modeling of occupants in frontal impacts, International Journal of Crashworthiness 14, 323-337.

[10] van der Laan, E.P., Heemels, W., Luijten, H., Veldpaus, F.E., Steinbuch, M., 2010. Reference governors for controlled belt restraint systems. Vehicle System Dynamics 48, 831–850.

[11] Bose, D., Crandall, J. R., Untaroiu, C. D., & Maslen, E. (2008, September). Influence of pre-collision occupant properties on the injury response during frontal collision. In IRCOBI Conf.

[12] Ostling, M., Eriksson, L., Forman, J. (2023) Need for injury criteria targets to address high exposure, low-severity frontal crashes. Proc. International Research Council on the Biomechanics of Impact.

[13] Bosma, F., van Hooijdonk, P., Tyssens, M., Kietlinski, K., & Unger, M. (2017). A Simulation Study on the Effect of AEB on Injuries on 50% Occupants. In 25th International Technical Conference on the Enhanced Safety of Vehicles (ESV) National Highway Traffic Safety Administration.

[14] Mertz, H. J., & Dalmotas, D. J. (2007). Effects of shoulder belt limit forces on adult thoracic protection in frontal collisions (51 (2007), pp. 361-380). In Stapp car crash journal. Proceedings of the 51st Stapp car crash conference, 29-31 October 2007, San Diego, California.

[15] Brumbelow, M. L., Baker, B. C., & Nolan, J. M. (2007, June). Effects of seat belt load limiters on driver fatalities in frontal crashes of passenger cars. In Proceedings of 20th International Technical Conference on the Enhanced Safety of Vehicles (pp. 07-0067).

[16] Perez-Rapela, D., Forman, J. L., Huddleston, S. H., & Crandall, J. R. (2020). Methodology for vehicle safety development and assessment accounting for occupant response variability to human and non-human factors. Computer methods in biomechanics and biomedical engineering, 24(4), 384-399.

[17] Wu, J., Cao, L. B., Zhang, R. F., & Hu, J. W. (2012). Model Development and Robust Optimal Design of Occupant Restraint System. In Advanced Materials Research (Vol. 538, pp. 2794-2797). Trans Tech Publications Ltd.

[18] Hu, J., Wu, J., Klinich, K. D., Reed, M. P., Rupp, J. D., & Cao, L. (2013). Optimizing the rear seat environment for older children, adults, and infants. Traffic injury prevention, 14(sup1), S13-S22.

[19] Hu, J., Flannagan, C. A., Bao, S., McCoy, R. W., Siasoco, K. M., & Barbat, S. (2015). Integration of active and passive safety technologies—a method to study and estimate field capability. Stapp Car Crash J, 59, 269-296.

[20] Rawska, K., Gepner, B., Shaw, G., & Kerrigan, J. R. (2018). Overview of a combined computational–experimental evaluation for the assessment of panoramic sunroof impact characteristics for ejection mitigation. Traffic Injury Prevention, 19(sup2), S96-S102.

[21] Bollapragada, V. (2019). The Influence of Disabling Injuries on the Design of the Vehicle Front End for Pedestrian Safety. PhD Dissertation, University of Virginia (available: https://libraetd.lib.virginia.edu/public_view/kp78gg99r).

[22] Forman, J., Kulkarni, S., Rapela, D. P., Mukherjee, S., Panzer, M., & Hallman, J. (2022, June). A method for thoracic injury risk function development for human body models. In IRCOBI Conference. Porto, Portugal (pp. 12-15).

[23] Poplin, G. S., McMurry, T. L., Forman, J. L., Ash, J., Parent, D. P., Craig, M. J., ... & Crandall, J. (2017). Development of thoracic injury risk functions for the THOR ATD. Accident Analysis & Prevention, 106, 122-130.

[24] Carroll, J., Adolph, T., Chauvel, C., Labrousse, M., Trosseille, X., Pastor, C., ... & Hynd, D. (2010). Overview of serious thorax injuries in European frontal car crash accidents and implications for crash test dummy development. In Proceedings of IRCOBI Conference (pp. 217-234).

[25] Kroell, C. (1971). Impact tolerance and response of the human thorax. In Proc. 15th Stapp Car Crash Conference, 1971 (pp. 84-134).

[26] Kroell, C. K., Schneider, D. C., & Nahum, A. M. (1974). Impact tolerance and response of the human thorax II. SAE Transactions, 3724-3762.

[27] Horsch, J. D., & Schneider, D. (1988). Biofidelity of the Hybrid III Thorax in high-velocity frontal impact. SAE transactions, 169-176.

[28] Yoganandan, N., Pintar, F. A., Kumaresan, S., Haffiner, M., & Kuppa, S. (1997). Impact biomechanics of the human thorax-abdomen complex. International journal of crashworthiness, 2(2), 219-228.

[29] Hardy, W. N., Schneider, L. W., & Rouhana, S. W. (2001). Abdominal impact response to rigid-bar, seatbelt, and airbag loading. Stapp car crash journal, 45, 1-32.

[30] Shaw, G., Lessley, D., Bolton, J., & Crandall, J. (2004). Assessment of the THOR and Hybrid III crash dummies: Steering wheel rim impacts to the upper abdomen (No. 2004-01-0310). SAE Technical Paper.

[31] Kent, R., Lessley, D., & Sherwood, C. (2004). Thoracic response to dynamic, non-impact loading from a hub, distributed belt, diagonal belt, and double diagonal belts. Stapp car crash journal, 48, 495.

[32] Salzar, R. S., Bass, C. R., Lessley, D., Crandall, J. R., Kent, R. W., & Bolton, J. R. (2009). Viscoelastic response of the thorax under dynamic belt loading. Traffic injury prevention, 10(3), 290-296.

[33] Kemper, A. R., Kennedy, E. A., McNally, C., Manoogian, S. J., Stitzel, J. D., & Duma, S. M. (2011). Reducing chest injuries in automobile collisions: rib fracture timing and implications for thoracic injury criteria. Annals of biomedical engineering, 39(8), 2141-2151.

[34] Cesari, D., & Bouquet, R. (1994). Comparison of Hybrid III and human cadaver thorax deformations loaded by a thoracic belt. SAE transactions, 1633-1644.

[35] Forman, J., Kent, R., Ali, T., Crandall, J., Bostrom, O., & Haland, Y. (2005). Biomechanical considerations for the optimisation of an advanced restraint system: assessing the benefit of a second shoulder belt. In IRCOBI Conference on the Biomechanics of Impact.

[36] Kleinbaum, D. G., & Klein, M. (2002). Logistic Regresion for Correlated Data: GEE. In: Logistic Regression. Statistics for Biology and Health. Springer, New York, NY. https://doi.org/10.1007/0-387-21647-2_11

[37] Bouquet, R., Ramet, M., Bermond, F., & Cesari, D. (1994, May). Thoracic and pelvis human response to impact. In Proc. 14th International Technical Conference on the Enhanced Safety of Vehicles (Vol. 1, pp. 100-109).

[38] Neathery, R. F. (1974). Analysis of chest impact response data and scaled performance recommendations. SAE Transactions, 3763-3779.

[39] Nahum, A. M., Gadd, C. W., Schneider, D. C., & Kroell, C. K. (1970). Deflection of the Human Thorax Under Sternal Impact (No. 700400). SAE Technical Paper.

[40] Nahum, A. M., Schneider, D. C., & Kroell, C. K. (1975). Cadaver skeletal response to blunt thoracic impact. SAE Transactions, 3160-3177.

[41] Vezin, P., Bruyère, K., & Bermond, F. (2001, June). Comparison of head and thorax cadaver and Hybrid III responses to a frontal sled deceleration for the validation of a car occupant mathematical model. In 17th International Technical Conference on the Enhanced Safety of Vehicles (ESV) (pp. 10-p).

[42] Vezin, P., Bruyere-Garnier, K., & Bermond, F. (2002, September). Human response to a frontal sled deceleration. In IRCOBI Conference on the Biomechanics of Impact (pp. pp-323).

[43] Arbogast, K. B., Balasubramanian, S., Seacrist, T., Maltese, M. R., Garcia-Espana, J. F., Hopely, T., ... & Higuchi, K. (2009). Comparison of kinematic responses of the head and spine for children and adults in low-speed frontal sled tests. Stapp car crash journal, 53, 329.

[44] Ewing, C. L., Thomas, D. J., Lustick, L., Muzzy, W. H. I., Willems, G., & Majewski, P. L. (1976). Effect of duration, rate of onset and peak sled acceleration on the dynamic response of the human head and neck. In Proceedings: Stapp Car Crash Conference (Vol. 20, pp. 3-41). Society of Automotive Engineers SAE.

[45] Schoeneburg, R., Baumann, K. H., Fehring, M., Ag, D., & Cars, M. (2011, June). The efficiency of PRE-SAFE systems in pre-braked frontal collision situations. In Proceedings of the 22nd ESV Conference (pp. 11-0207).

[46] Happee, R., Hoofman, M., Van den Kroonenberg, A. J., Morsink, P., & Wismans, J. S. H. M. (1998). A mathematical human body model for frontal and rearward seated automotive impact loading. SAE transactions, 2720-2734.

Appendix A: Brief Illustrations of Load cases Simulated in this Study

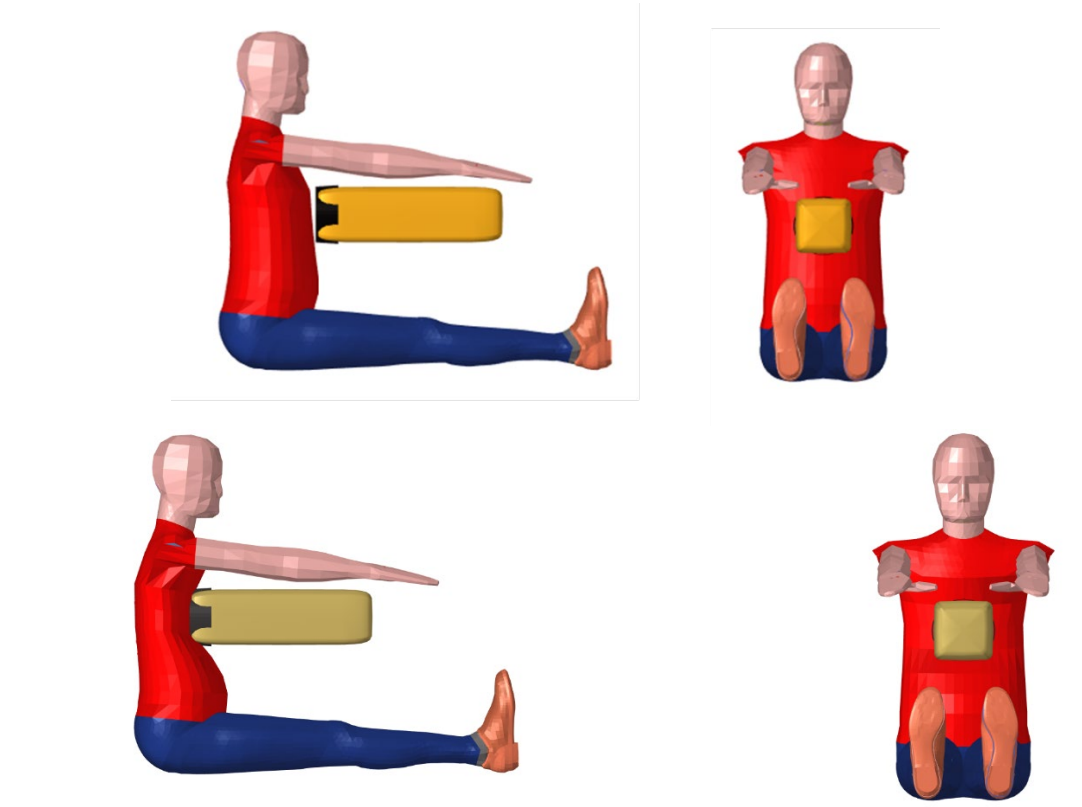

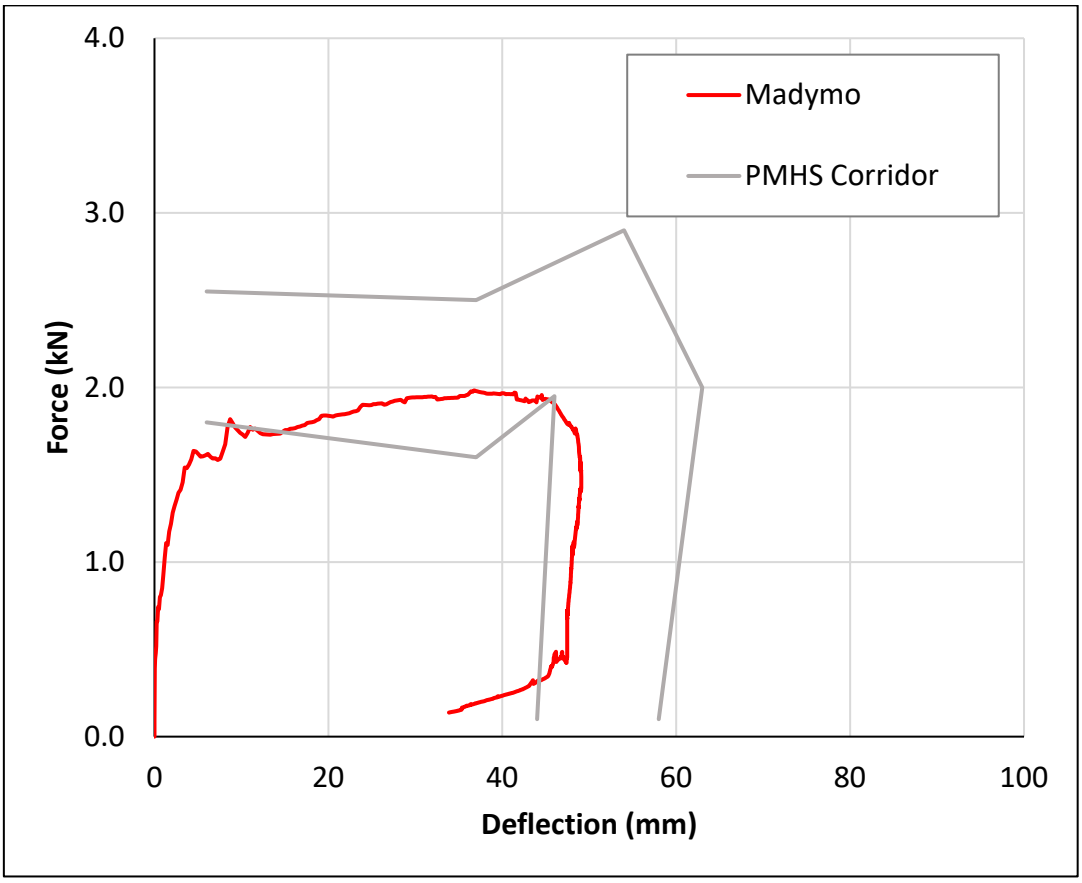

Fig. A1. Hub impactor case of Kroell et al. [25-26] (top-undeformed, bottom-deformed)

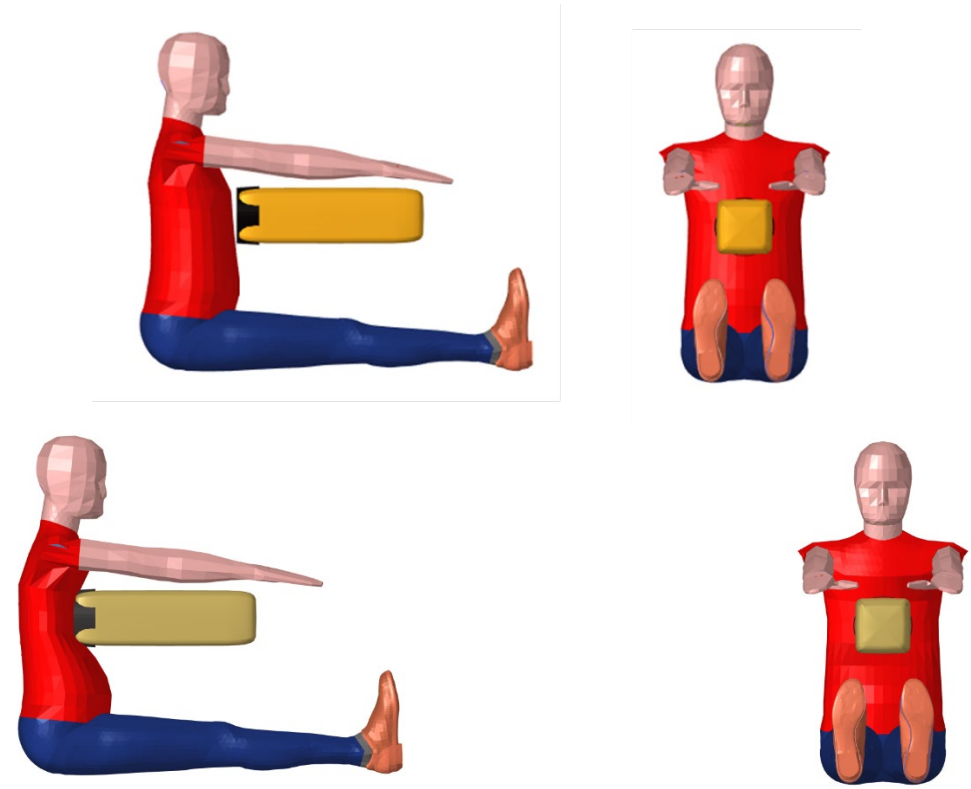

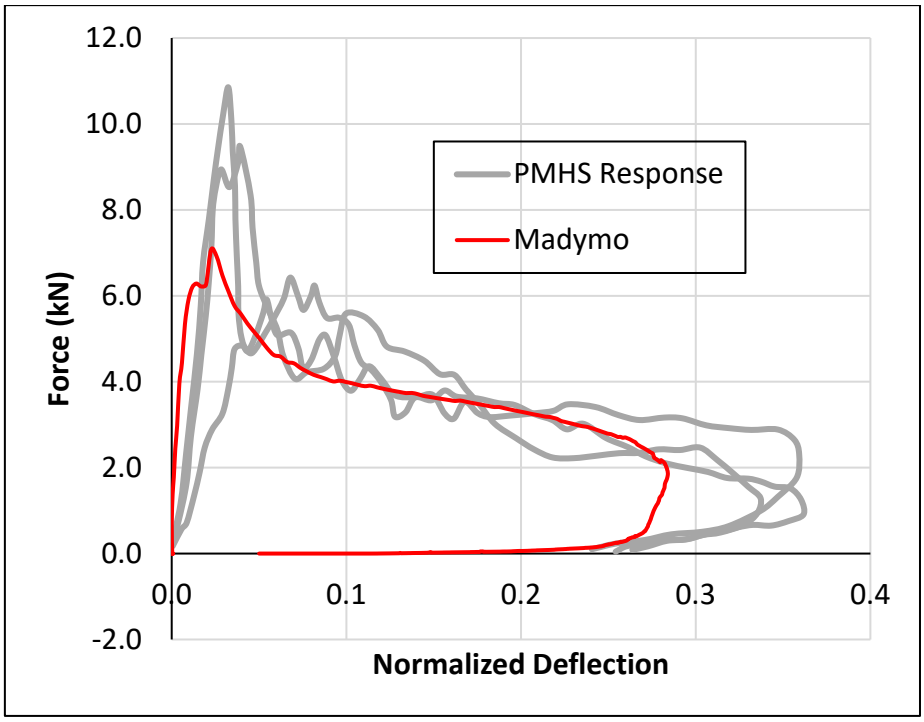

Fig. A2. Hub impactor case of Horsch et al. [27] (top-undeformed, bottom-deformed)

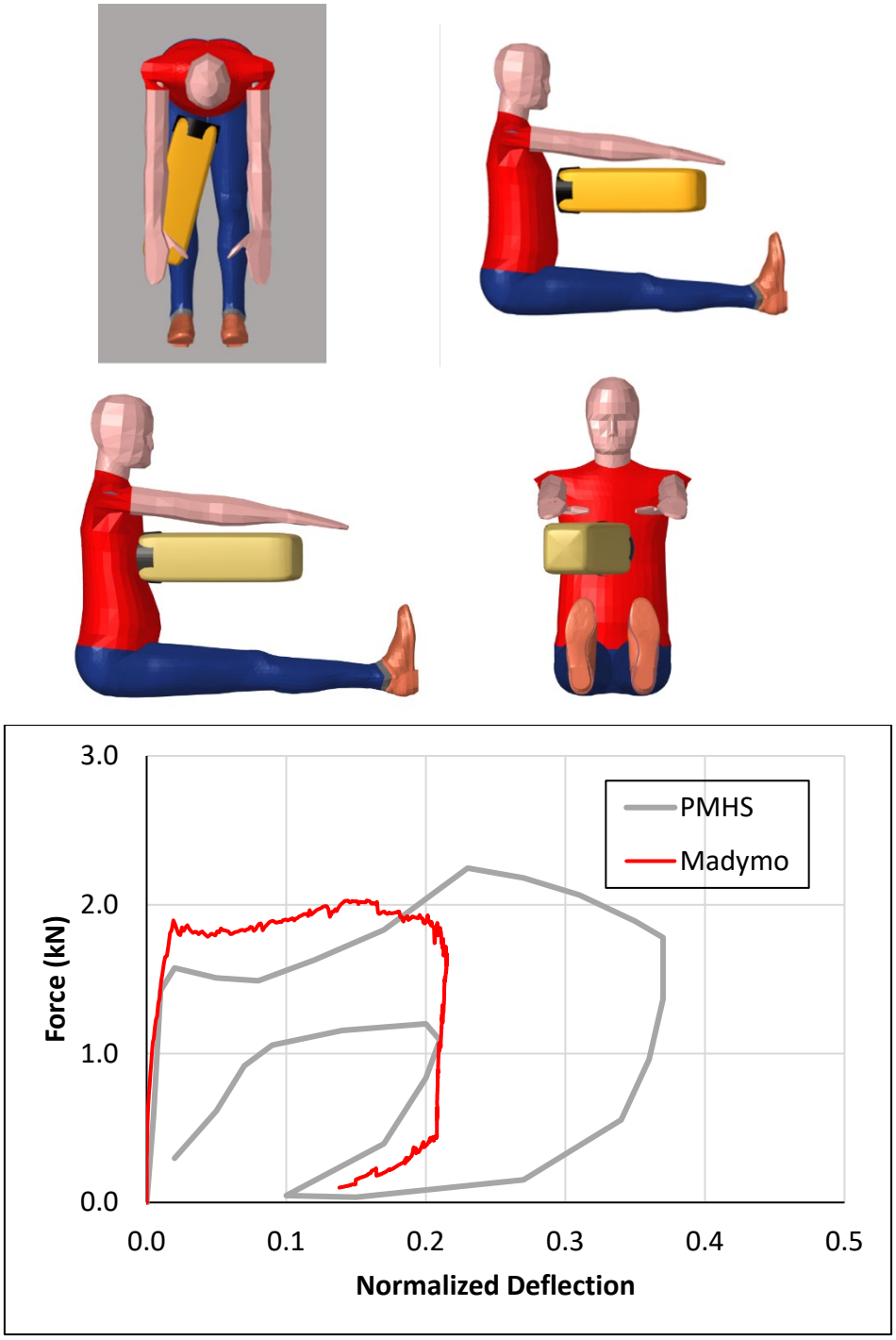

Fig. A2: Oblique hub impactor case of Yoganandan et al. [28] (top-undeformed, bottom-deformed)

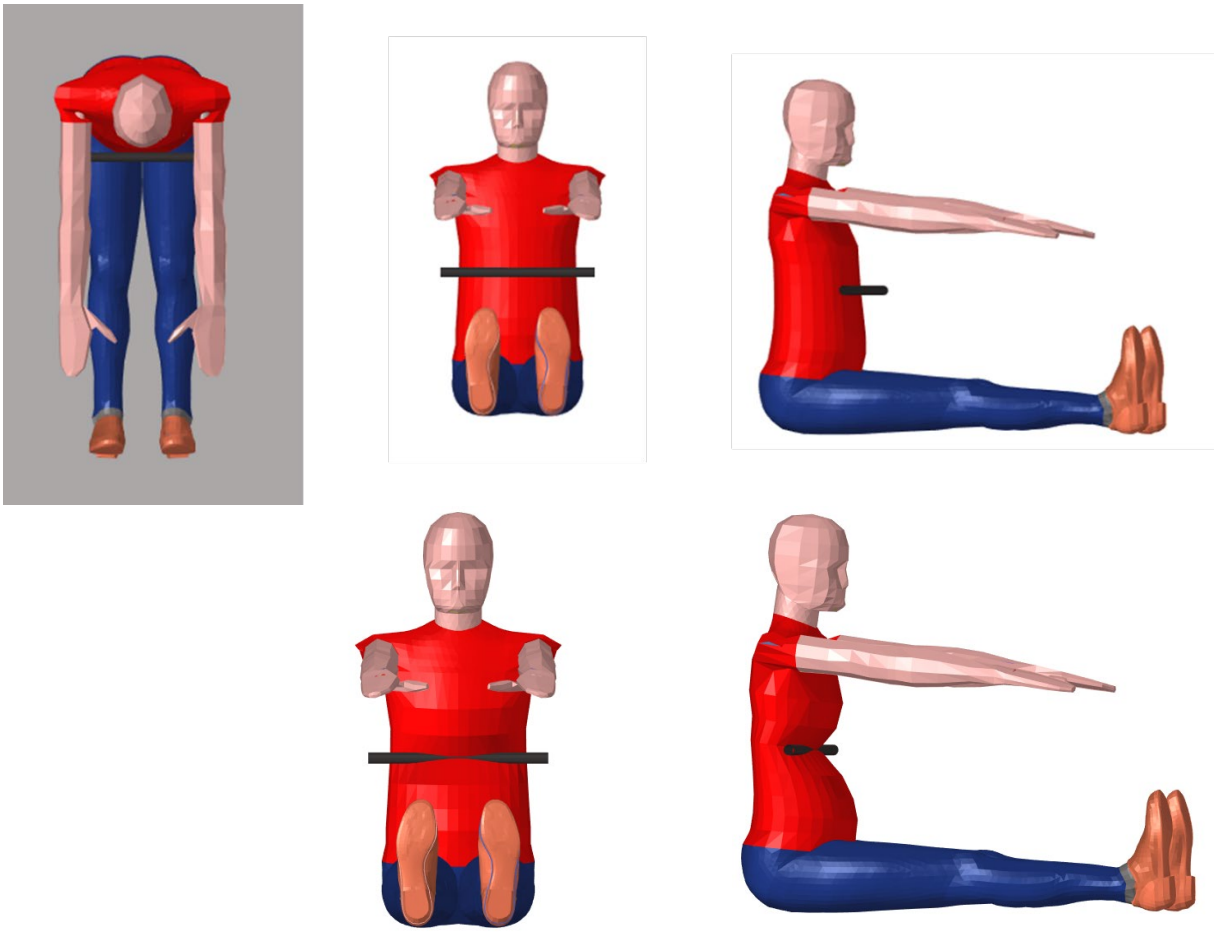

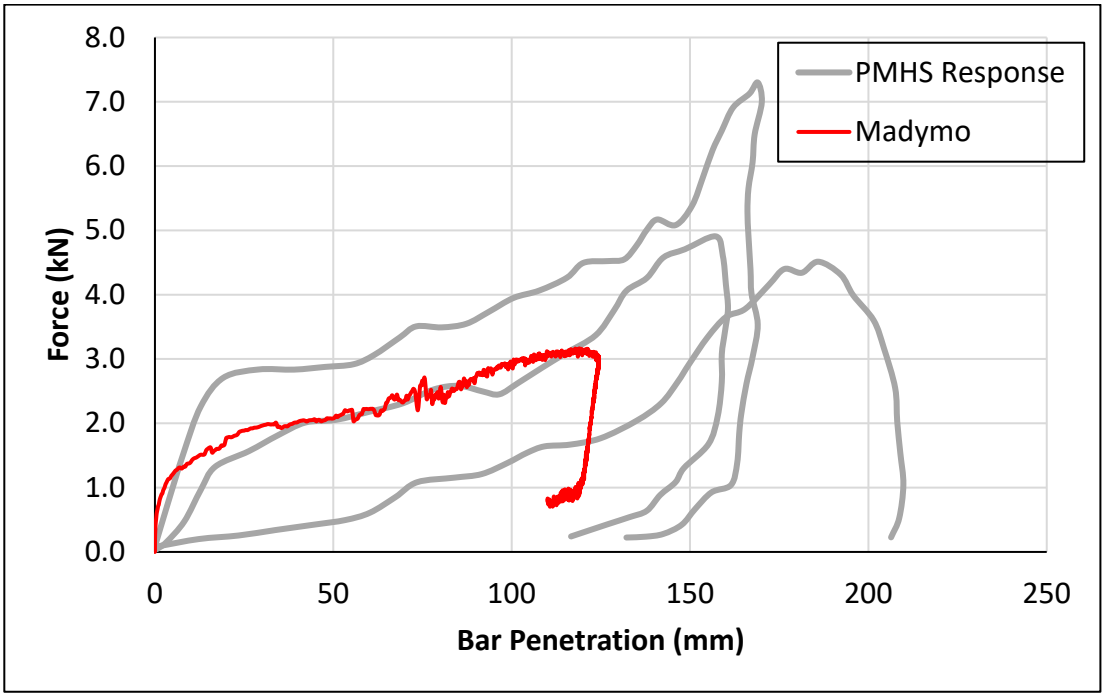

Fig. A3. Rigid rod impactor case of Hardy et al. [29] (top-undeformed, bottom-deformed)

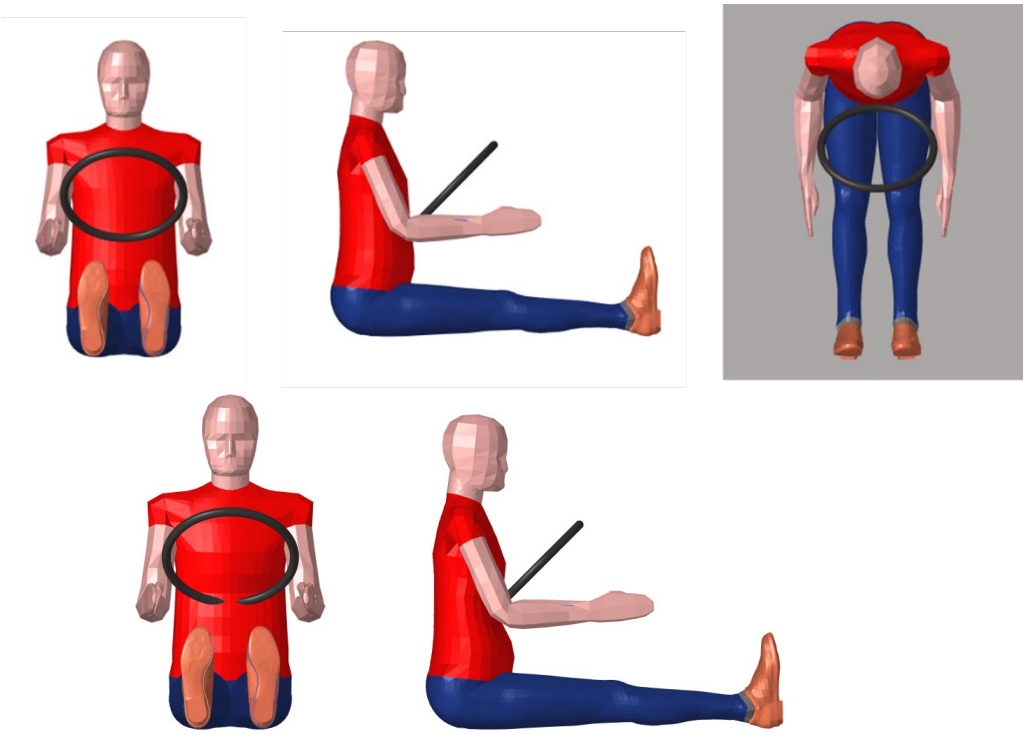

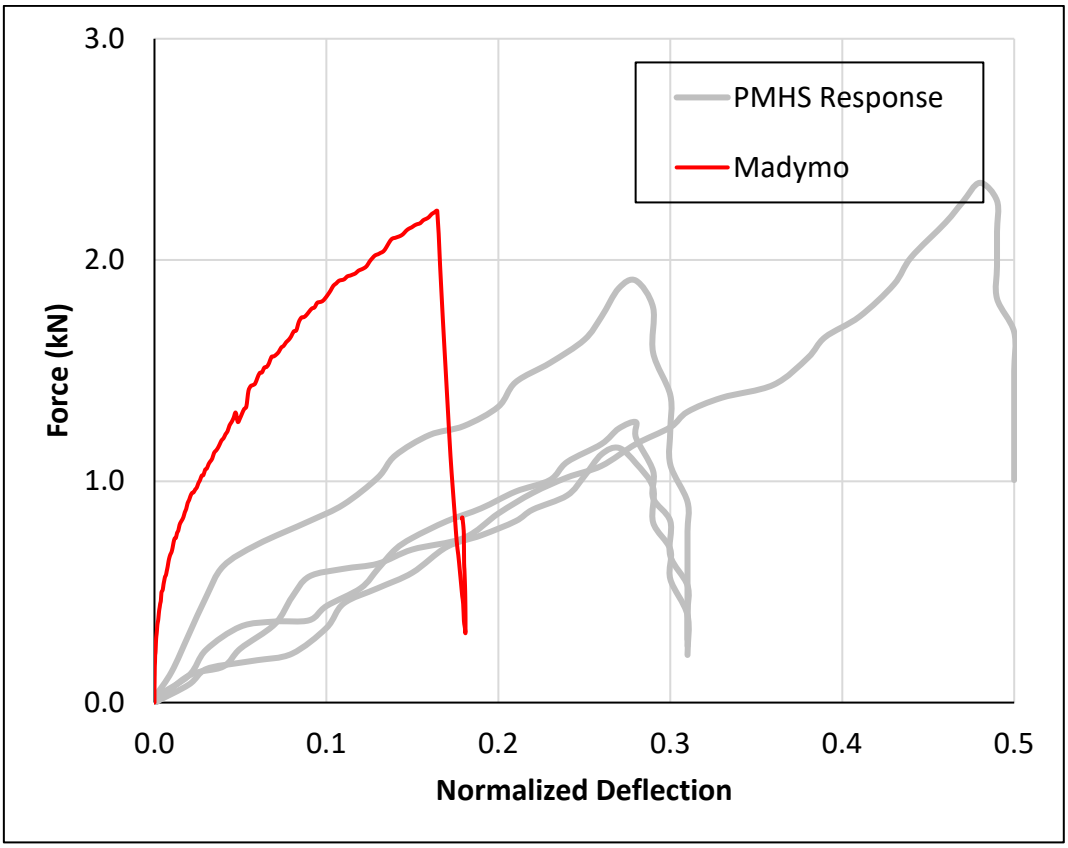

Fig. A4. Steering wheel rim impactor case of Shaw et al. [30]. (top-undeformed, bottom-deformed)

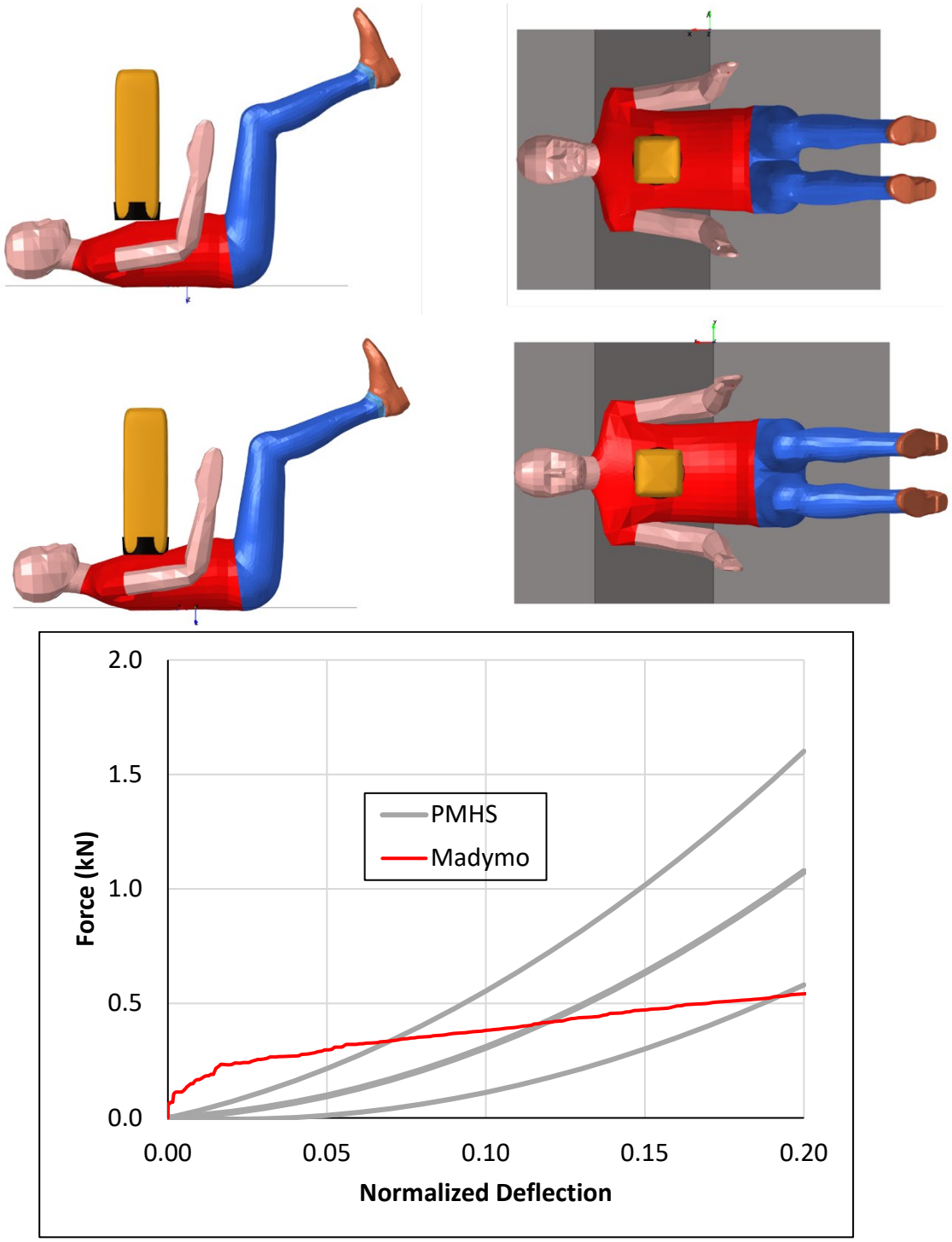

Fig. A5. Table-top hub loading case of Kent et al. [31]. (top-undeformed, bottom-deformed)

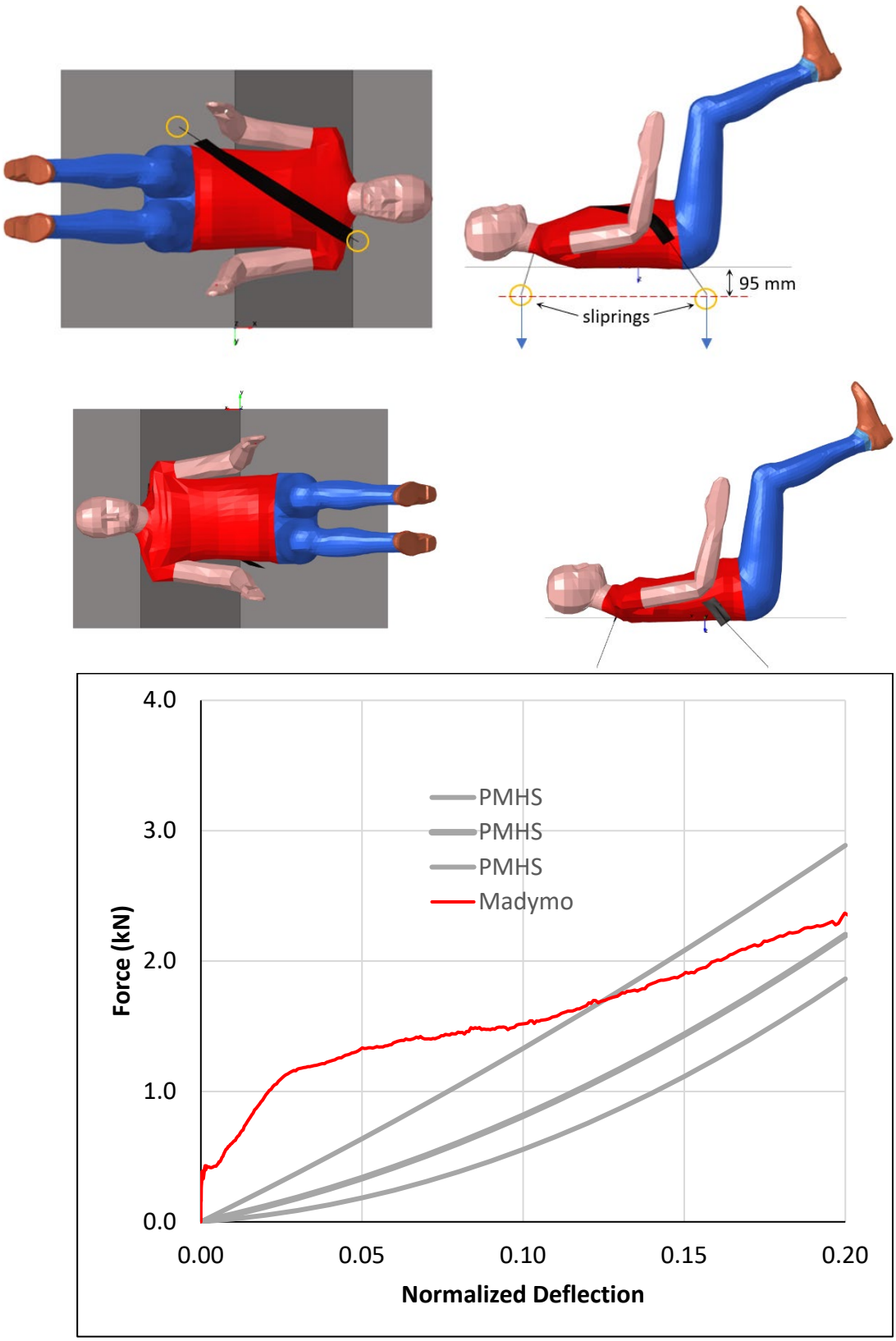

Fig. A6. Table-top single-diagonal-belt case of Kent et al. [31]

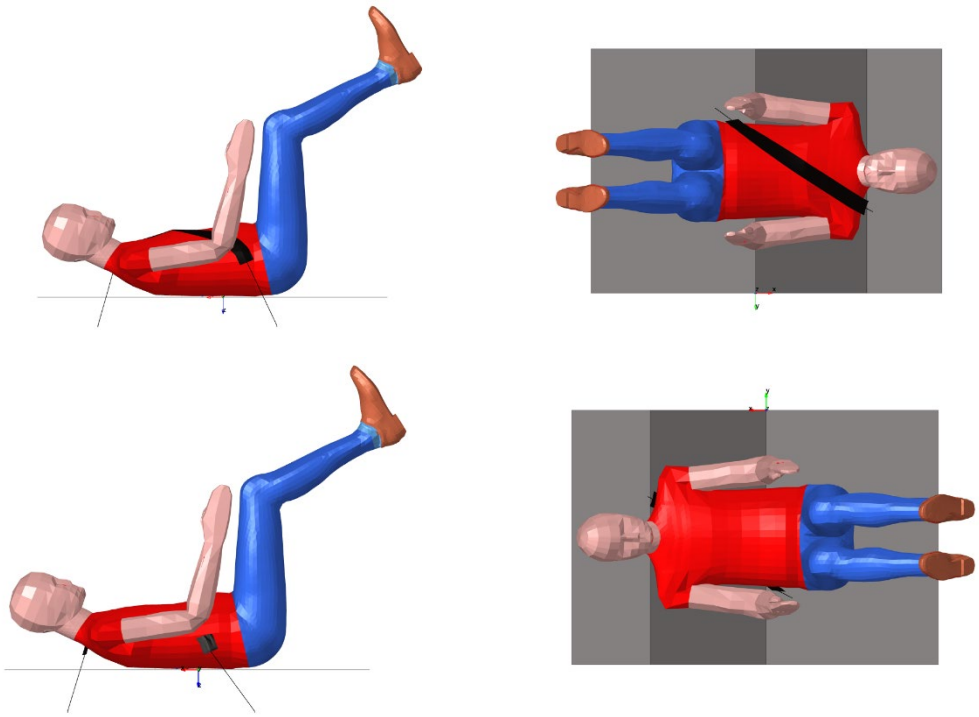

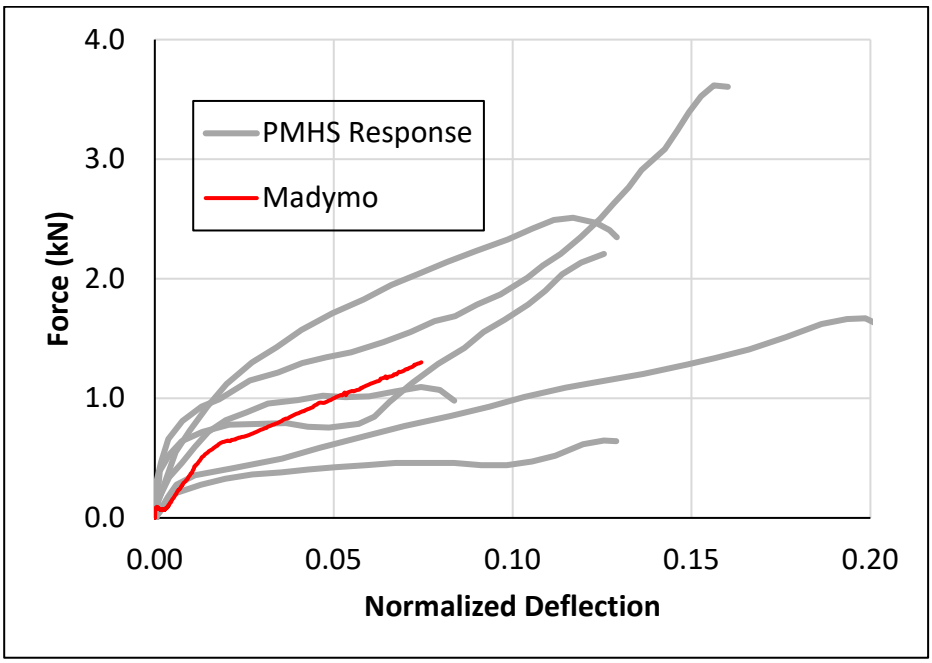

Fig. A7. Table-top single-diagonal-belt case of Salzar et al. [32]. (top-undeformed, bottom-deformed)

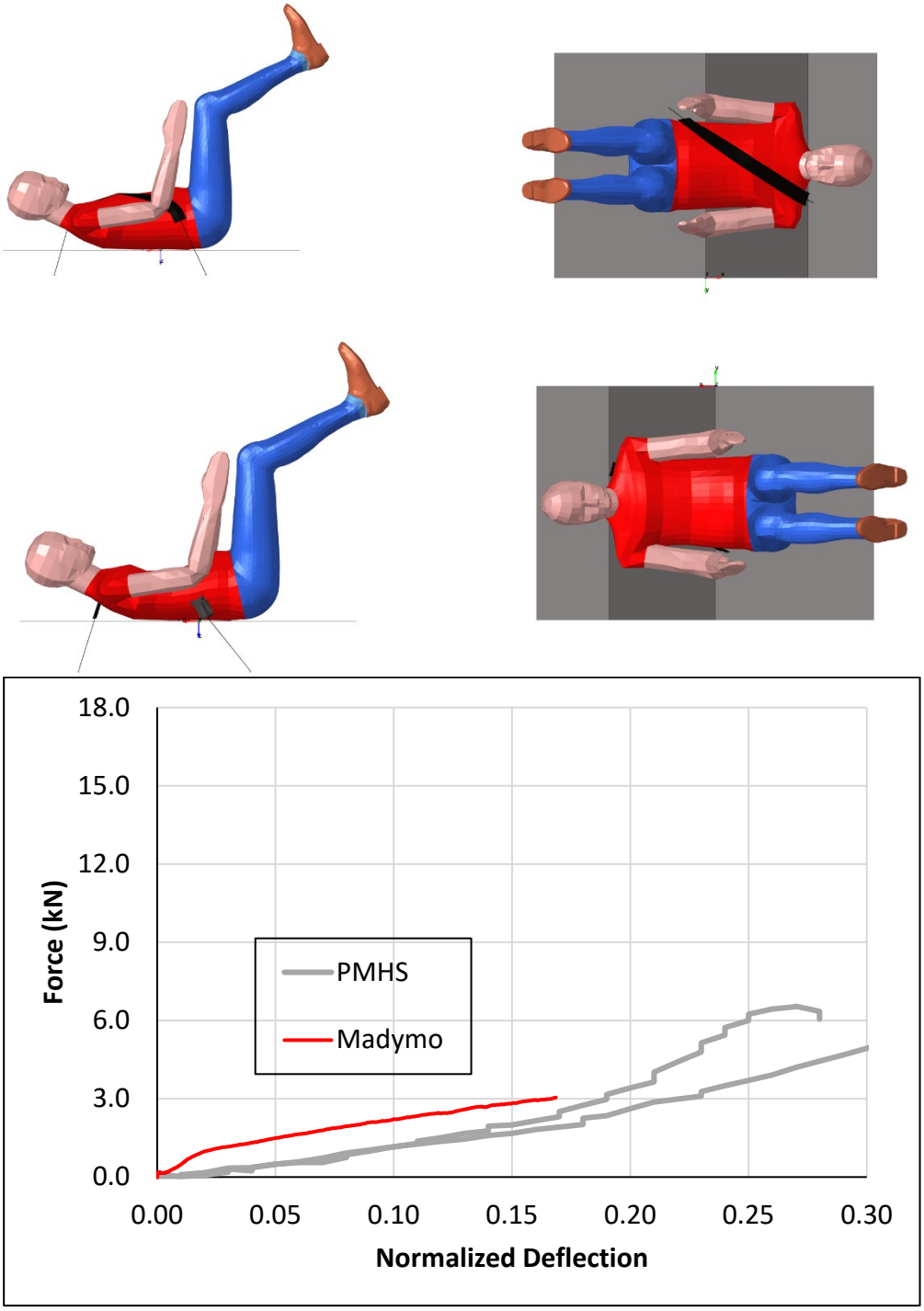

Fig. A8. Table-top single-diagonal-belt case of Kemper et al. [33]. (top-undeformed, bottom-deformed)

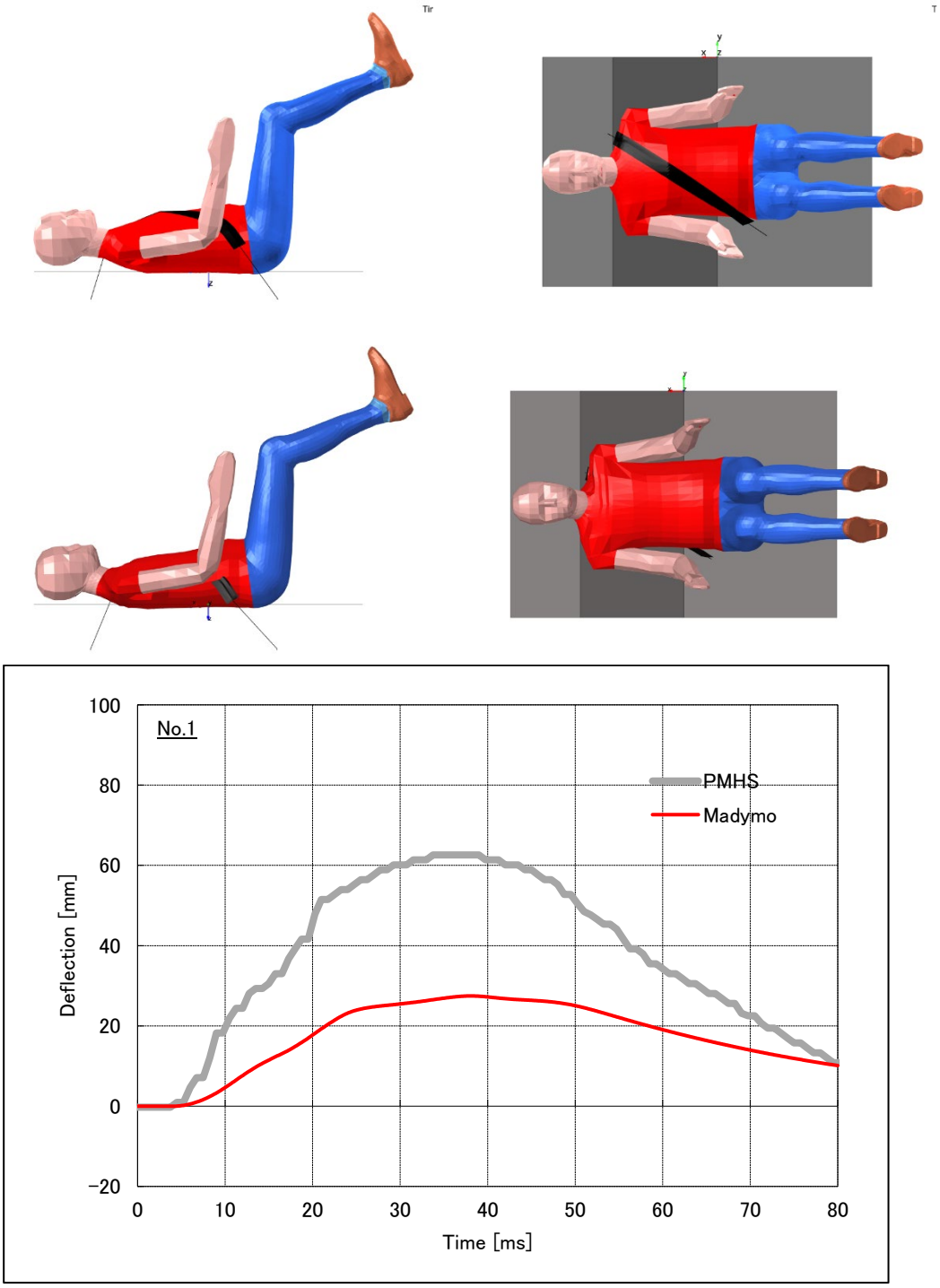

Fig. A9. Table-top single-diagonal-belt case of Cesari et al. [34]. (top-undeformed, bottom-deformed)

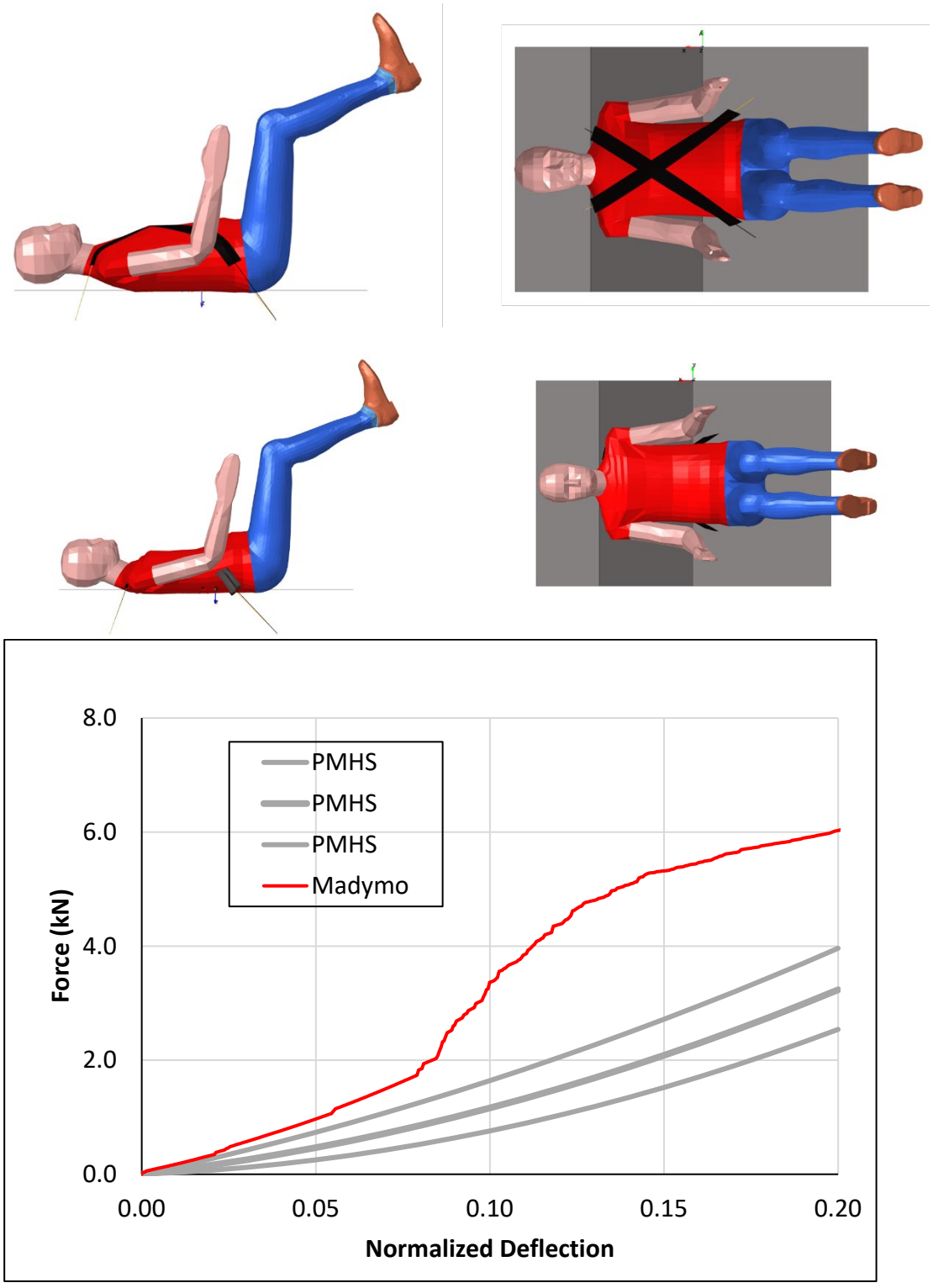

Fig. A10. Table-top double-diagonal-belt case of Kent et al. [31]. (top-undeformed, bottom-deformed)

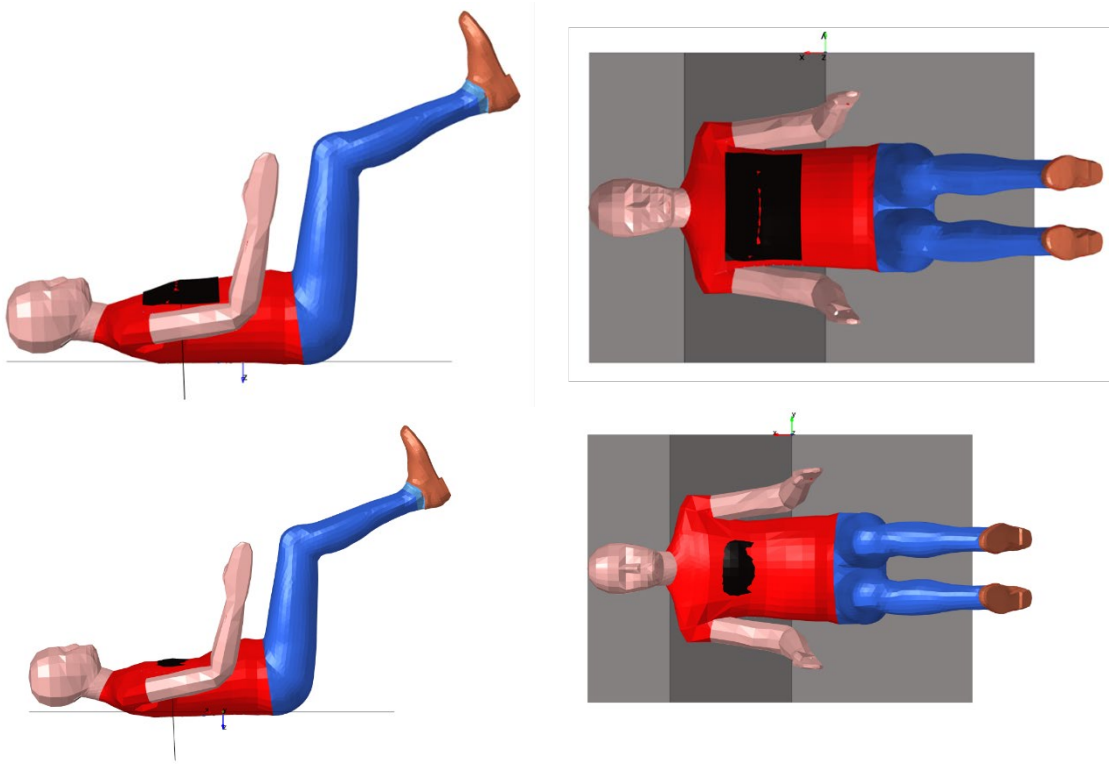

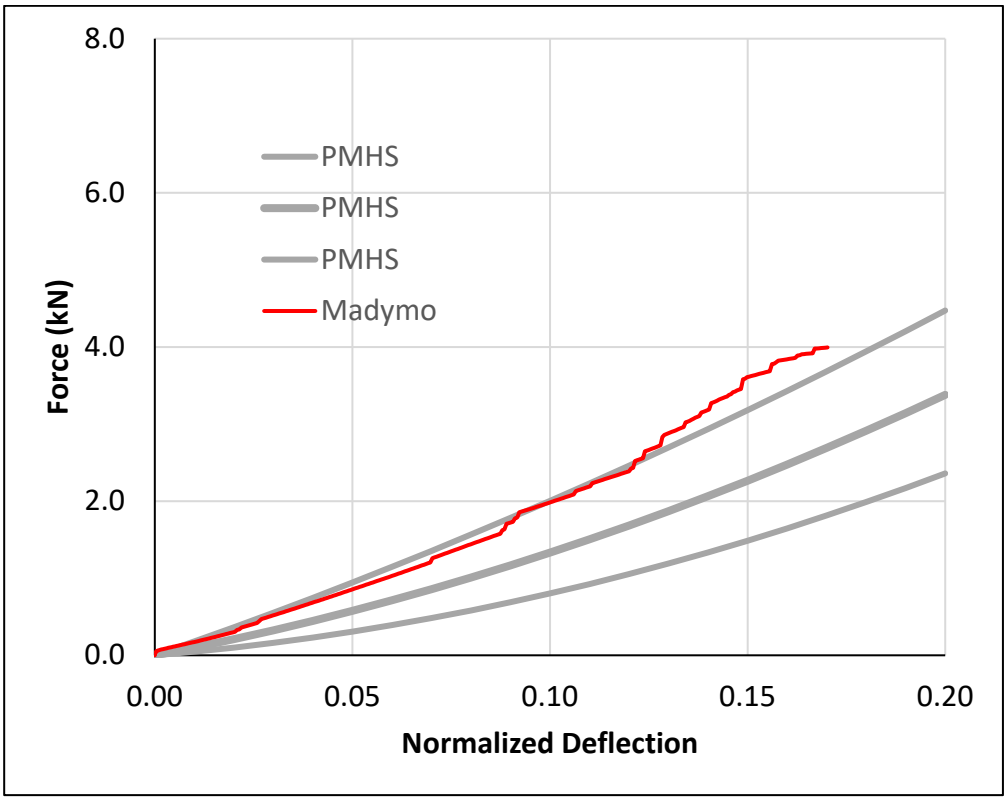

Fig. A11. Table-top distributed belt case of Kent et al. [31]. (top-undeformed, bottom-deformed)

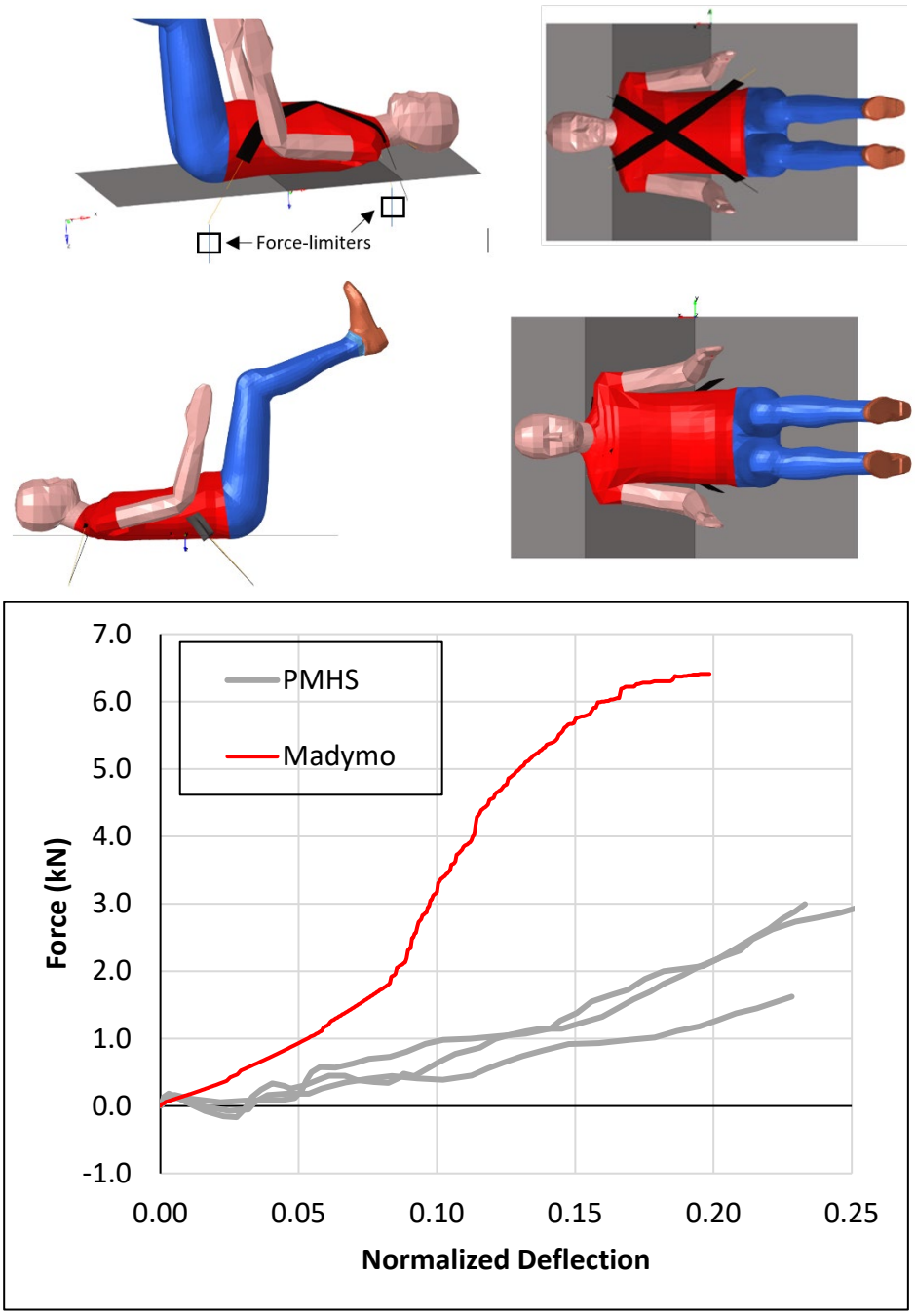

Fig. A12. Table-top double-diagonal-belt case of Forman et al. [35], with force-limiting in one of the belts (to result in differential force application). (top-undeformed, bottom-deformed)

Appendix B:

TABLE B I
PMHS DETAILS AND INJURY INFORMATION FOR ALL TESTS REFERENCED IN THIS STUDY, AND MAX. CHEST DEFLECTION FROM EACH MATCHED SIMULATION

Load Case	PMHS_ID	Test_ID	Age	Sex	Height (cm)	Weight (kg)	Total Rib Fractures	3+ Rib Fractures	7+ Rib Fractures	Max Def. (m)
01 Horsch 1988	119FM	218	69	M	178.3	65	11	1	1	0.070
	121FM	219	66	M	185.5	68.2	6	1	0	0.068
	123FM	220	58	M	173.7	72.3	7	1	1	0.066
02 Yoganadan 1997	1	1	72	M	170	82	5	1	0	0.047
	2	2	81	M	175	63	4	1	0	0.052
	3	3	84	M	168	68	0	0	0	0.050
	4	4	86	M	170	56	2	0	0	0.054
	5	5	62	M	174	61	3	1	0	0.053
	6	6	70	M	169	91	4	1	0	0.045
	7	7	68	M	178	83	11	1	1	0.047
03 Hardy 2001	28800	GI5	65	F	164	61	13	1	1	0.133
	29084	GI10	64	M	180	65	20	1	1	0.175
	29115	GI11	74	M	168	75	16	1	1	0.128
04 Shaw 2004	2000-FRM-135	Cad1	63	M	172.6	69.1	3	1	0	0.040
	2002-FRM-159	Cad2	66	M	166.5	65.9	2	0	0	0.040
	2001-FRM-149	Cad3	40	M	158.3	43.1	1	0	0	0.040
	2002-FRM-161	Cad4	61	M	181.7	65.8	16	1	1	0.040
05 Kroell 1974	11FF	60	60	F	160	58.9	11	1	1	0.076
	12FF	61	67	F	162.5	62.6	24	1	1	0.088
	13FM	65	81	M	167.6	76.2	21	1	1	0.084
	14FF	66	76	F	157.5	57.6	7	1	1	0.091
	15FM	69	80	M	165.1	53	13	1	1	0.090
	18FM	76	78	M	175.3	65.7	16	1	1	0.082
	19FM	77	19	M	NA	65.7	1	0	0	0.082
	20FM	79	29	M	180.3	56.7	0	0	0	0.086
	21FF	82	45	F	172.7	68.5	19	1	1	0.082
	22FM	83	72	M	182.9	74.8	17	1	1	0.078
	23FF	85	58	F	162.5	61.2	23	1	1	0.089
	24FM	86	65	M	182.9	81.6	6	1	0	0.103
	25FM	87	65	M	167.6	54.4	18	1	1	0.092
	26FM	88	75	M	172.7	63.5	0	0	0	0.033
	28FM	90	54	M	182.9	68	0	0	0	0.037
	30FF	92	52	F	156	40.8	3	1	0	0.155
	31FM	93	51	M	183	74.8	15	1	1	0.113
	32FM	94	75	M	171	54.4	21	1	1	0.125
	34FM	96	64	M	178	59	13	1	1	0.095

05 Kroell 1974	36FM	99	52	M	183	74.8	7	1	1	0.077
	37FM	104	48	M	179	73.9	10	1	1	0.110
	42FM	171	61	M	183	54.4	0	0	0	0.066
	43FM	172	59	M	178	54.4	4	1	0	0.065
	45FM	177	64	M	181	64	11	1	1	0.065
	46FM	178	46	M	178	94.8	0	0	0	0.073
	48FM	182	69	M	170	64.4	0	0	0	0.064
	50FM	186	66	M	181	59.9	13	1	1	0.068
	51FM	187	60	M	185	82.1	0	0	0	0.053
	52FM	188	65	M	175	51.7	12	1	1	0.071
	53FM	189	75	M	174	77.1	3	1	0	0.062
	54FF	190	49	F	163	37.2	7	1	1	0.093
	55FF	191	46	F	177	81.2	8	1	1	0.100
	56FM	192	65	M	177	73.9	3	1	0	0.059
	58FM	196	68	M	179	68.9	4	1	0	0.059
	60FM	200	66	M	180	79.4	9	1	1	0.052
	62FM	202	76	M	174	50.3	10	1	1	0.068
	63FM	203	53	M	183	88	5	1	0	0.076
	64FM	204	72	M	163	63	6	1	0	0.085
06 Kent 2004 Hub	147	Cadve42	63	F	161	45	0	0	0	0.020
	145	Cadve62	54	M	192	87.7	0	0	0	0.031
	145	Cadve64	54	M	192	87.7	6	1	0	0.048
	155	Cadve67	71	F	166	54.4	0	0	0	0.019
	170	Cadve87	75	M	178	65	0	0	0	0.031
	173	Cadve103	67	F	162	57.2	0	0	0	0.025
	178	Cadve127	73	M	182	80.7	0	0	0	0.033
	177	Cadve146	79	F	161	47.6	0	0	0	0.017
	177	Cadve149	79	F	161	47.6	24	1	1	0.045
	176	Cadve152	85	F	157	58.2	0	0	0	0.020
	182	Cadve171	80	F	157	65.3	0	0	0	0.021
	157	Cadve179	55	F	168	74.4	0	0	0	0.033
	186	Cadve197	58	F	178	61.2	0	0	0	0.011
	186	Cadve201	58	F	178	61.2	8	1	1	0.043
	188	Cadve203	71	M	173	85.3	0	0	0	0.031
	187	Cadve217	54	M	178	112.7	1	0	0	0.025
	190	Cadve230	79	M	173	73.5	0	0	0	0.016
	189	Cadve248	79	M	159	56.7	0	0	0	0.022
07 Kent 2004 Dist.	147	Cadve45	63	F	161	45	0	0	0	0.016
	145	Cadve57	54	M	192	87.7	0	0	0	0.022
	155	Cadve73	71	F	166	54.4	0	0	0	0.019
	170	Cadve96	75	M	178	65	0	0	0	0.019
	170	Cadve98	75	M	178	65	11	1	1	0.026
	173	Cadve100	67	F	162	57.2	0	0	0	0.022
	178	Cadve120	73	M	182	80.7	0	0	0	0.025

07 Kent 2004 Dist.	177	Cadve143	79	F	161	47.6	0	0	0	0.011
	176	Cadve155	85	F	157	58.2	0	0	0	0.018
	182	Cadve167	80	F	157	65.3	0	0	0	0.013
	157	Cadve176	55	F	168	74.4	0	0	0	0.029
	186	Cadve195	58	F	178	61.2	0	0	0	0.007
	188	Cadve207	71	M	173	85.3	0	0	0	0.017
	187	Cadve221	54	M	178	112.7	0	0	0	0.020
	190	Cadve232	79	M	173	73.5	0	0	0	0.014
	189	Cadve250	79	M	159	56.7	0	0	0	0.014
08 Kent 2004 SB	147	Cadve50	63	F	161	45	1	0	0	0.009
	145	Cadve54	54	M	192	87.7	0	0	0	0.014
	155	Cadve69	71	F	166	54.4	1	0	0	0.013
	170	Cadve93	75	M	178	65	1	0	0	0.019
	173	Cadve105	67	F	162	57.2	0	0	0	0.018
	178	Cadve124	73	M	182	80.7	1	0	0	0.026
	177	Cadve139	79	F	161	47.6	1	0	0	0.010
	176	Cadve159	85	F	157	58.2	0	0	0	0.010
	176	Cadve161	85	F	157	58.2	8	1	1	0.031
	182	Cadve163	80	F	157	65.3	0	0	0	0.009
	182	Cadve174	80	F	157	65.3	22	1	1	0.029
	157	Cadve182	55	F	168	74.4	1	0	0	0.017
	186	Cadve192	58	F	178	61.2	1	0	0	0.005
	188	Cadve209	71	M	173	85.3	1	0	0	0.015
	187	Cadve225	54	M	178	112.7	0	0	0	0.013
	187	Cadve228	54	M	178	112.7	1	0	0	0.021
	190	Cadve234	79	M	173	73.5	0	0	0	0.010
	189	Cadve246	79	M	159	56.7	0	0	0	0.012
09 Kent 2004 DB	155	Cadve71	71	F	166	54.4	0	0	0	0.019
	170	Cadve90	75	M	178	65	0	0	0	0.027
	173	Cadve107	67	F	162	57.2	0	0	0	0.026
	178	Cadve122	73	M	182	80.7	1	0	0	0.033
	177	Cadve141	79	F	161	47.6	0	0	0	0.010
	176	Cadve157	85	F	157	58.2	0	0	0	0.017
	182	Cadve165	80	F	157	65.3	0	0	0	0.014
	157	Cadve184	55	F	168	74.4	0	0	0	0.026
	157	Cadve188	55	F	168	74.4	27	1	1	0.037
	186	Cadve190	58	F	178	61.2	0	0	0	0.009
	188	Cadve211	71	M	173	85.3	0	0	0	0.022
	187	Cadve223	54	M	178	112.7	0	0	0	0.017
	190	Cadve236	79	M	173	73.5	0	0	0	0.017
09 Kent 2004 DB	190	Cadve240	79	M	173	73.5	12	1	1	0.023
	189	Cadve242	79	M	159	56.7	0	0	0	0.018
10 Kemper 2011	1	01Male	65	M	183	76.8	14	1	1	0.033
	2	02Female	69	F	155	50.9	8	1	1	0.047

11 Salzar 2009	412	12	62	M	175	68	0	0	0	0.009
	412	13	62	M	175	68	0	0	0	0.020
	413	22	54	M	175	68	0	0	0	0.005
	413	23	54	M	175	68	0	0	0	0.012
	419	33	31	M	193	90	0	0	0	0.013
	419	34	31	M	193	90	0	0	0	0.020
12 Forman 2005	207	cadve205	67	F	160	49.9	0	0	0	0.028
	207	cadve206	67	F	160	49.9	0	0	0	0.025
	207	cadve207	67	F	160	49.9	0	0	0	0.021
	207	cadve208	67	F	160	49.9	0	0	0	0.020
	207	cadve209	67	F	160	49.9	0	0	0	0.023
	207	cadve210	67	F	160	49.9	0	0	0	0.020
	207	cadve212	67	F	160	49.9	8	1	1	0.032
	194	cadve217	38	F	170	94.8	0	0	0	0.019
	194	cadve218	38	F	170	94.8	0	0	0	0.020
	194	cadve219	38	F	170	94.8	0	0	0	0.024
	194	cadve220	38	F	170	94.8	0	0	0	0.015
	194	cadve221	38	F	170	94.8	0	0	0	0.025
	194	cadve222	38	F	170	94.8	0	0	0	0.023
	194	cadve223	38	F	170	94.8	0	0	0	0.026
	194	cadve225	38	F	170	94.8	0	0	0	0.026
	195	cadve227	67	F	173	58.9	0	0	0	0.024
	195	cadve229	67	F	173	58.9	0	0	0	0.025
	195	cadve230	67	F	173	58.9	0	0	0	0.018
	195	cadve231	67	F	173	58.9	0	0	0	0.018
	195	cadve232	67	F	173	58.9	0	0	0	0.018
	195	cadve233	67	F	173	58.9	0	0	0	0.021
	195	cadve234	67	F	173	58.9	0	0	0	0.022
	195	cadve238	67	F	173	58.9	21	1	1	0.051
13 Cesari 1990	THC11	thc11	47	F	170	92.5	8	1	1	0.026
	THC12	thc12	17	F	164	58.5	0	0	0	0.027
	THC13	thc13	86	F	160	43	2	0	0	0.015
	THC14	thc14	69	M	173	82	17	1	1	0.030
	THC15	thc15	60	M	177	69	3	1	0	0.024
	THC16	thc16	59	M	170	62	4	1	0	0.034
	THC17	thc17	71	M	177	75	7	1	1	0.027
	THC18	thc18	67	M	174	47	6	1	0	0.036
	THC19	thc19	83	F	155	43	4	1	0	0.026
	THC20	thc20	70	M	160	63	18	1	1	0.023
13 Cesari 1990	THC62	thc62	72	M	183	53	4	1	0	0.014
	THC65	thc65	71	M	170	41	10	1	1	0.029
	THC69	thc69	40	M	183	56	1	0	0	0.024
	THC75	thc75	60	M	160	44.5	6	1	0	0.021
	THC77	thc77	64	F	164	49.5	6	1	0	0.014

	THC79	thc79	43	M	186	54	3	1	0	0.023
	THC93	thc93	63	M	176	56	10	1	1	0.022

Appendix C:

TABLE C I
IMPACTOR MASSES AND VELOCITIES FOR IMPACTOR CASES

Load Case	PMHS_ID	Test_ID	Test Impactor Mass (kg)	Test Impactor Initial Velocity (m/s)	Scaled impactor mass for Madymo v3.3 (kg)
01_[15]	119FM	218	4.25	13.4	4.92
	121FM	219	4.25	13.4	4.69
	123FM	220	4.25	13.4	4.43
02_ [16]	1	1	23.5	4.3	21.58
	2	2	23.5	4.3	28.09
	3	3	23.5	4.3	26.02
	4	4	23.5	4.3	31.60
	5	5	23.5	4.3	29.01
	6	6	23.5	4.3	19.45
	7	7	23.5	4.3	21.32
03_ [17]	28800	GI5	48	6	59.25
	29084	GI10	48	8.9	55.61
	29115	GI11	48	6.2	48.19
04_ [18]	2000-FRM-135	Cad1	64	4	69.74
	2002-FRM-159	Cad2	64	4	73.13
	2001-FRM-149	Cad3	64	4	111.81
	2002-FRM-161	Cad4	64	4	73.24
05_ [14]	11FF	60	19.5	6.3	24.93
	12FF	61	22.8	7.2	27.43
	13FM	65	22.8	7.4	22.53
	14FF	66	22.8	7.3	29.81
	15FM	69	23.6	6.9	33.53
	18FM	76	23.6	6.7	27.05
	19FM	77	23.6	6.7	27.05
	20FM	79	23.6	6.7	31.34
	21FF	82	23.6	6.8	25.94
	22FM	83	23.6	6.7	23.76
	23FF	85	19.5	7.7	23.99
	24FM	86	22.8	9.6	21.04
	25FM	87	5.5	13.8	7.61
	26FM	88	1.8	11.1	2.13
	28FM	90	1.6	14.5	1.77
	30FF	92	15.9	13.23	29.34
	31FM	93	23.04	10.19	23.19
	32FM	94	22.86	9.92	31.64
	34FM	96	18.96	8.23	24.20
	36FM	99	18.96	7.2	19.09
	37FM	104	22.86	9.83	23.29
	42FM	171	22.86	4.87	31.64
	43FM	172	22.86	4.83	31.64
	45FM	177	23	5.05	27.06
	46FM	178	19.28	7.33	15.31
	48FM	182	10.43	7.06	12.20

05_ [14]	50FM	186	10.43	7.29	13.11
	51FM	187	10.43	6.66	9.57
	52FM	188	10.43	7.2	15.19
	53FM	189	22.95	5.23	22.41
	54FF	190	19.55	6.71	39.57
	55FF	191	19.55	9.92	18.13
	56FM	192	10.43	6.93	10.63
	58FM	196	10.43	6.75	11.40
	60FM	200	22.95	4.34	21.76
	62FM	202	9.98	6.93	14.94
	63FM	203	23	6.93	19.68
	64FM	204	23	6.93	27.49